

https://dspace.org/

Automotive heater core for off-design conditions

Bhaiyat, Taahir Ibrahim

2023
https://hdl.handle.net/10539/36946

Downloaded from a DSpace repository. https://dspace.org/

AUTOMOTIVE HEATER CORE FOR OFF–DESIGN CONDITIONS

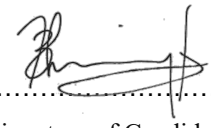
Taahir Ibrahim Bhaiyat

A dissertation submitted to the Faculty of Engineering and the Built Environment, University of the Witwatersrand, in fulfilment of the requirements for the degree of Master of Science in Engineering.

Johannesburg, 2023

DECLARATION

I declare that this dissertation is my own unaided work. It is being submitted to the Degree of Master of Science to the University of the Witwatersrand, Johannesburg. It has not been submitted before for any degree or examination to any other University.



……

(Signature of Candidate)

4th day of March, 2023

(day) (month) (year)

ABSTRACT

This dissertation presents the overall heat transfer performance of a louvered fin-and-tube heater core and a newly developed "lattice porous" heater core, each operating under uniform and non-uniform incident flow-fields. Specific emphasis is placed on the physical mechanisms pertaining to their differences in heat transfer rates, based on thermal and hydraulic dispersion characteristics of the cores. The variation of heat transfer rate with airstream flowrate is experimentally detailed in a typical range applicable to Automotive Climate Control System (ACCS) units (i.e., $58.8 \leq Re_{lp} \leq 361$). It has been demonstrated that a non-uniform airstream incident on a louvered fin-and-tube core reduces heat transfer to the airstream, while a non-uniform airstream incident on a lattice porous core enhances heat transfer to the airstream. This is because concentrated regions of momentum in a non-uniform incident airstream are fully dispersed, laterally, throughout a lattice porous core, thereby increasing surface interaction between the core and the airstream, as well as increasing flow mixing.

To my beloved father, Ibrahim, and my angel mother, Shehnaz, for their infinite patience and support.

ACKNOWLEDGEMENTS

I am extremely grateful for the assistance and mentorship from my dissertation supervisors Prof. Tongbeum Kim and Dr. Michael Atkins. Their constant feedback, direction, support, and commitment were critical to the completion this work. I extend my gratitude to Prof. Tian Jian Lu at the Nanjing University of Aeronautics and Astronautics, for providing the unique opportunity to manufacture test samples at his Key Laboratory for Multifunctional Lightweight Materials and Structures in Nanjing, PR China, and to Mr. Yan Yan Liu, for enabling my stay in Nanjing. I thank Mr. Sjouke Schekman and Mr. Andrew Heyndrichs for their expert assistance with laboratory equipment and engineering advice throughout my time at Wits. I acknowledge the efforts of Mr. Shaun Riekert and his excellent team at the North-West Engineering Laboratory including Mr. Rowen Parumal and Mr. Buti, without whom this research would not have been possible. I thank Hanon Systems in Dajeon, South Korea, for their commercial test samples and valued industry advice.

CONTENTS **Page**

DECLARATION i
ABSTRACT ii
DEDICATION iii
ACKNOWLEDGEMENTS iv
LIST OF FIGURES vii
LIST OF TABLES ix
LIST OF SYMBOLS x

1 INTRODUCTION 1
1.1 Background 1
1.2 Literature Review 7
1.2.1 Louvered fin-and-tube core operation at design conditions 7
1.2.2 Performance deterioration at off-design conditions 11
1.2.3 Preventing off-design performance deterioration with aerodynamic anisotropy 14
1.3 Research Objectives and Methods 16
1.4 Publications 17

2 EXPERIMENTS 18
2.1 Test Rig and Setups 18
2.1.1 Water heating circuit 19
2.1.2 Design performance test setup 20
2.1.3 Off-design performance (ACCS unit) test setup 20
2.1.4 Simulated off-design performance test setups 21
2.1.5 Temperature measurements 22
2.1.6 Airstream flowrate and velocity profile measurements 22
2.1.7 Surface flow visualization (Oil-dye technique) 25
2.1.8 Temperature mapping (IR Thermography) 25
2.2 Heater Core Geometries 25
2.3 Data Processing 27
2.3.1 Epsilon-NTU method for unmixed cross-flow 27
2.3.2 Air-side heat transfer coefficient 29
2.3.3 Fin efficiencies for louvered and cylindrical fin geometries 29
2.3.4 Tube conduction resistances 30
2.3.5 Water-side heat transfer coefficient 31
2.3.6 Colburn j-factor and selection of a characteristic length 31
2.4 Uncertainty Analysis 33
2.4.1 Absolute uncertainties of measurement instruments 33
2.4.2 Propagation of absolute uncertainties through data processing 34

3 DISCUSSION OF RESULTS 35
3.1 Thermo-Fluidic Performance of a Louvered Fin-and-Tube Heater Core 35
3.1.1 At design conditions (verification of experiments) 35
3.1.2 At off-design conditions (inside an ACCS) 37
3.1.3 At simulated ACCS unit conditions 38
3.2 Hydraulic Dispersion 43
3.2.1 In a louvered fin-and-tube core 43
3.2.2 In a lattice porous core (influence of aerodynamic anisotropy) 44
3.3 Thermo-Fluidic Performance of a Lattice Porous Core 45
3.3.1 At design and off-design conditions 45
3.3.2 The role of staggered fin-functioning ligaments in thermal dispersion 47
3.4 Summary 47

4 CONCLUSIONS 50

5 RECOMMENDATIONS FOR FUTURE WORK 52

6 REFERENCES 53

LIST OF FIGURES

Figure 1. Overall layout of heat exchanger components: (a) inside a vehicle hood [4], (b) inside an ACCS unit. 2

Figure 2. Heater core with hot coolant water flowing through its tubes and an ambient airstream impinging its surface. 3

Figure 3. Common compact heat exchanger fin geometries [9]. 4

Figure 4. Performance data for plate-fin surface heat exchangers from Kays & London [3]: (a) Colburn j-factor vs Re, (b) friction factor vs Re. 5

Figure 5. Airflow directions through louvered fins at low and high Reynolds numbers. 5

Figure 6. Schematic representation of the experimental setup used to characterize heater core performance at design conditions. 6

Figure 7. Geometry of an ACCS unit's duct system showing the presence of off-design conditions in practice: (a) non-uniform and non-parallel incident airflow, (b) flow area changes upstream and downstream of the core. 6

Figure 8. Flattening of the Stanton number curve, indicating transition from duct flow to flat-plate flow, in two representative louvered fin-and-tube cores studied by Achaichia & Cowell [19]. 9

Figure 9. Typical off-design conditions previously studied: (a) blockage screen position upstream of a core, (b) blockage screens studied by Datta et al. [15] and Blecich [16], (c) effect of a linear blockage screen on the velocity profile of an incident airstream, (d) common configurations with "A" type and inclined fin-and-tube cores in central air-conditioning systems. 13

Figure 10. Typical flow paths and exit velocity profile for louvered fins with non-uniform incident velocity profile (adopted from Bellows [27]). 14

Figure 11. Flow paths and velocity profiles for porous media with non-uniform incident velocities (adopted from Barratt & Kim [32]): (a) Low porosity & high lateral dispersion, (b) Critical porosity, (c) High porosity & low lateral dispersion. 15

Figure 12. Schematic of hot water supply and measurement system for waterflow through the header tubes of a test core. 18

Figure 13. Blowdown rectangular wind-tunnel showing the transverse (x), lateral (y), and longitudinal (z) directions for: (a) a louvered fin-and-tube heater core positioned in the test section, (b) a lattice porous heater core positioned in the test section. 19

Figure 14. Automotive climate control system (ACCS) unit used in this study to characterize the combined off-design conditions typically found in automobile air-conditioning systems: (a) Frontal view, (b) Side view. 21

Figure 15. Schematic representation of wind tunnel modifications used in this study to simulate individual and combined off-design conditions found in the ACCS unit: (a) A wedge obstruction placed immediately upstream of the heater core and no downstream ducting (i.e., half-ACCS unit), (b) An upstream wedge obstruction and upward ducting downstream of the heater core (i.e., full-ACCS unit). 22

Figure 16. Volume flowrate supplied by the ACCS unit's centrifugal fan at four step input power settings; Low, Medium, Medium-high and High. 23

Figure 17. Schematic of wind-tunnel test section showing the downstream traverse plane for a Pitot tube..... 24

Figure 18. Cut-away views showing core dimensions: (a) Louvered fin-and-tube core and unit cell (adopted from Shah & Sekulic [1]), (b) Circular tube bank without fin ligaments, (c) Circular tube bank with staggered fin ligaments (i.e., a lattice porous core). 26

Figure 19. Design performance of a louvered fin-and-tube heater core: (a) Nusselt number (Nu_{lp}) variation with Reynolds number (Re_{lp}), (b) Colburn j-factor (j) variation with Reynolds number (Re_{lp}), relative to previous correlations..... 36

Figure 20. Comparison of thermal performance of a louvered fin-and-tube heater core operating under design and off-design conditions (i.e., inside the ACCS unit): (a) Variation of Nusselt numbers measured at design conditions ($Nu_{lp(Ref)}$) and off-design conditions ($Nu_{lp\ (ACCS)}$) with louver pitch-based Reynolds number (Re_{lp}), (b) Variation of $Nu_{lp(ACCS)}$ with Re_{lp}, normalized by $Nu_{lp(Ref)}$..... 37

Figure 21. Schematic representation of air flow inside an ACCS unit without ducting downstream of the core (i.e., half-ACCS unit)..... 39

Figure 22. Influence of the wedge obstruction alone on the thermal performance of a louvered fin-and-tube heater core..... 39

Figure 23. Effect of an upstream wedge on the thermal performance of a louvered fin-and-tube heater core: (a) Velocity profiles for $Re_{lp} = 180$, measured at A = $0.3H$ upstream from the wedge and at B = $0.2H$ downstream from the heater core, (b) Infrared thermographs of the heater core showing the effect of non-uniform incident coolant flow on the temperature distribution of the core. 40

Figure 24. Flow visualization image showing separated flow marked by a bright region of accumulated dye particles..... 41

Figure 25. Combined influence of the wedge obstruction and downstream ducting on the thermal performance of a louvered fin-and-tube heater core..... 42

Figure 26. Schematic representation of separated and recirculating flow regions inside an ACCS unit. 42

Figure 27. Velocity profiles measured at $0.75L_t$ downstream of a louvered fin-and-tube core with a wedge placed immediately upstream as indicated in the inset. 44

Figure 28. Lattice porous heater core: (a) Assembled core with header tubes, (b) Cut-away view in the x-z plane (A-A). 44

Figure 29. Velocity profiles $0.75L_t$ downstream of a lattice porous heater core with a wedge placed immediately upstream as indicated in the inset. 45

Figure 30. Overall thermal performance comparison between a louvered fin-and-tube core and a lattice porous core operating at off-design conditions, simulated by the half-ACCS wind tunnel configuration: (a) Normalized performance variation with Re_{Dh}, (b) Nusselt number variation with Re_{Dh}..... 46

Figure 31. Heat transfer in a lattice porous heater core: (a) Design and off-design thermal performance of a circular tube bank without horizontal fin-functioning ligaments, (b) Contribution of circular fin ligaments to the overall heat transfer in a lattice porous heater core..... 48

LIST OF TABLES

Table 1. Published heat transfer and friction factor correlations 10

Table 2. Volumetric flowrate based on speed settings, measured in the present study. 24

Table 3. Tubes and fins dimensions 26

Table 4: Absolute uncertainties of measurement instruments used in this study. 33

LIST OF SYMBOLS

A_a	Total air-side heat transfer surface area	m^2
A_w	Total water-side heat transfer surface area	m^2
A_t	Tube wall conduction surface area	m^2
b	Fin height	mm
C	Heat capacity rate	W/K
C_r	Heat capacity rate ratio	-
c_p	Specific heat capacity	J/kg-K
δ	Fin thickness	mm
D	Diameter	mm
D_h	Hydraulic diameter of the rectangular cooling channel	mm
d	Turbine meter diameter	mm
η_0	Surface efficiency	-
η_f	Fin efficiency	-
ε	Effectiveness	-
h	Heat transfer coefficient	W/m^2-K
H	Core height	mm
H_t	Flat tube height	mm
j	Colburn j-factor	-
k	Thermal conductivity	W/m-K
l_p	Louver pitch	mm
l_h	Louver height	mm
l_l	Fin ligament length	mm

L_t	Tube depth	mm
L_f	Fin depth	mm
$\dot{m}$	Mass flow rate	kg/s
μ	Dynamic viscosity	Pa · s
N_t	Number of tubes	-
NTU	Number of Transfer Units	-
Nu	Nusselt number	-
Pr	Prandtl number	-
P_f	Fin pitch	mm
$\dot{q}$	Heat transfer rate	W
Q	Flow rate	L/s
ρ	Density	kg/m^3
Re	Reynolds number	-
R	Overall thermal performance ratio	-
R_f	Fins thermal performance ratio	-
r	Tube rib thickness	mm
S_T	Transverse tube pitch	mm
S_L	Longitudinal tube pitch	mm
S_1	Deflection louver length	mm
S_2	Turnaround louver length	mm
θ	Louver angle	^{o}
t	Flat tube wall thickness	mm
T	Temperature	K

u	Local fluid velocity	m/s
u_m	Mean fluid velocity	m/s
U	Overall heat transfer coefficient	W/m^2-K
W	Core width	mm

Subscripts

a	Air
al	Aluminum
h	Hydraulic
in	Inlet
i	Inner
l	Ligament
min	Minimum
max	Maximum
out	Outlet
o	Outer
t	Tube
w	Water

1 INTRODUCTION

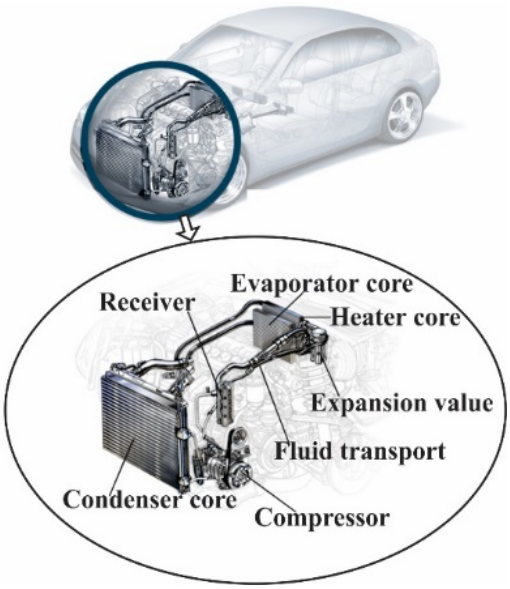
1.1 Background

Climate control systems are included in modern automobiles to make driving more comfortable. A heater core and an evaporator core are used in the system to distribute warmed and cooled air, respectively, to the passenger cabin. Fig. 1(a) shows that the evaporator core forms part of a refrigeration cycle, being connected to a compressor, a condenser, and an expansion valve through fluid transport hoses. The heater core is connected, also via hoses, to transport hot coolant from the engine. The temperature of an ambient airstream is adjusted by passing over either of the cores, before being directed toward the passenger cabin, due to hot coolant flowing through the heater core and cold refrigerant flowing through the evaporator core.

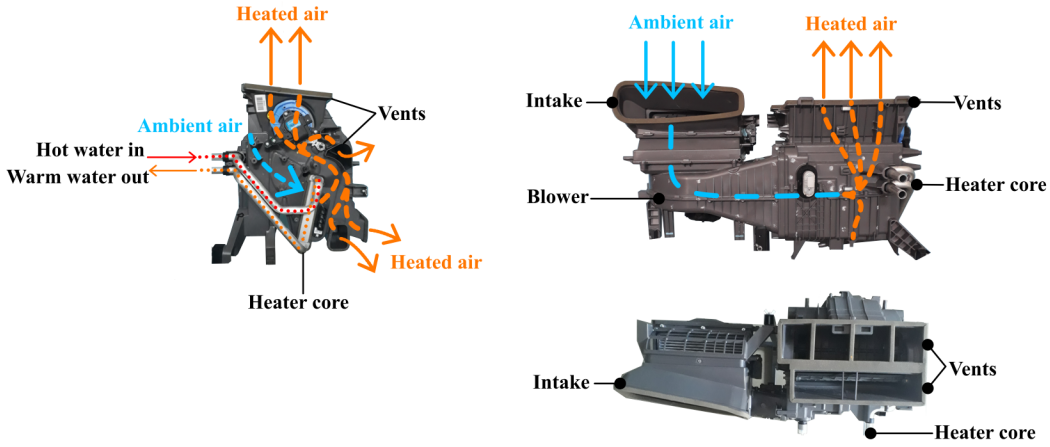
The heater and evaporator cores, including a blower, are packaged inside a compact unit, known as Automotive Climate Control System (ACCS), as shown in Fig 1(b). To heat up a passenger cabin, the blower initially draws an ambient airstream from the surroundings, through an intake duct. The ACCS's internal ducting then directs the airstream toward the heater core. It impinges the heater core surface, as shown in Fig. 2, and passes over the core's fins and tubes. In doing so, heat from the hot coolant (which enters the core's tubes via an inlet header) is convectively transferred to the airstream. First, the heated coolant from the engine warms the inner tube surface via internal convection. Conduction then causes the outer tube surface and the fins in contact with the tubes to heat up. Finally, heat is transferred to the airstream by external convection between the fin-and-tube surface and airflow. As a result, the coolant temperature drops while the airstream temperature rises. Several vents downstream of the heater core then guide the heated airstream into the passenger cabin, while the warm coolant travels from the outlet header to the vehicle's engine, where it warms up further before returning to the inlet header of the heater core.

To increase the overall heat transfer coefficient of a liquid-to-gas heat exchanger, such as the foregoing heater core, it is more effective to enhance convection on the gas side of the heat exchanger (i.e., the external convection), instead of enhancing either convection on the liquid side (i.e., the internal convection) or conduction through the heat exchanger material. This is because the thermal resistance of a gas is typically one or two orders of magnitude higher than that of a solid or a liquid [1-3]. To increase the rate of external convection, one may either increase the airstream flowrate or the external heat transfer surface area. Both techniques, to varying degrees, speed up the rate of heat transfer at the expense of higher skin friction drag - which causes increased pressure drop across the core [1, 3] and thus requires greater pumping power to overcome the frictional losses. On the one hand, increasing airstream flowrate increases heat transfer at a rate that varies with less than the first power of the airstream velocity, while raising drag by at least the square of the airstream velocity. On the other hand, increasing the external surface area results in proportional increases in both heat transfer and skin friction drag. Thus, if the pumping power available to the blower is

constrained, as in the case of an ACCS being a secondary vehicle component, it becomes necessary to reduce the airstream velocity and compensate for the decreased heat transfer rate with an extended heat transfer surface area. This is indeed the function of fins in several liquid-to-gas heat exchangers, which often have surface area densities exceeding 700 m^2/m^3 and are thus classified as *compact* heat exchangers [1].



(a)



(b)

Figure 1. Overall layout of heat exchanger components: (a) inside a vehicle hood [4], (b) inside an ACCS unit.

Compact heat exchangers typically consist of narrow airflow passages through the fins, in which small characteristic dimensions ensure low Reynolds numbers. Therefore, airflow through the passage is often laminar at realistic air flowrates and becomes fully developed (meaning that the boundary layers along the passage walls gradually increase in thickness until they eventually merge [5]) after a relatively short entrance length (L_e) according to $L_e/x \approx 0.06Re_x$ where x is the

characteristic length [6, 7]. As the boundary layers increase in thickness, within the entrance region, the temperature and velocity gradients near the passage walls correspondingly decrease, causing reduced heat transfer and skin friction drag respectively [2, 8]. Once the airflow is fully developed the temperature and velocity gradients remain constant with further increases in passage length [5]. To enhance convection at the fin surfaces, it is therefore necessary to combat increasing boundary layer thickness. Hence, interruptions to the fin surface are usually present. The laminar boundary layers close to the fin surface are destroyed by the interruptions, which frequently take the form of waviness, offset strips, perforations, or louvers, as shown in Fig. 3. Consequently, the thermal and hydraulic boundary layers must restart periodically, which limits the maximum thickness of the boundary layers. In this way, fin surface interruptions passively maintain large temperature and velocity gradients near the fin surface to effect increased heat transfer and skin friction drag [1, 2]. Usually, there is also an accompanied increase in flow mixing and form drag, i.e., drag induced by a low-pressure region formed in the wake of an interruption, which are responsible for further increases in heat transfer and pressure drop, respectively. The size of the wake behind an interruption, and thus the magnitude of the heat transfer and form drag produced, is a function of the interruption geometry and manufacturing precision. Therefore, each interruption promotes distinct heat transfer and pressure drop characteristics.

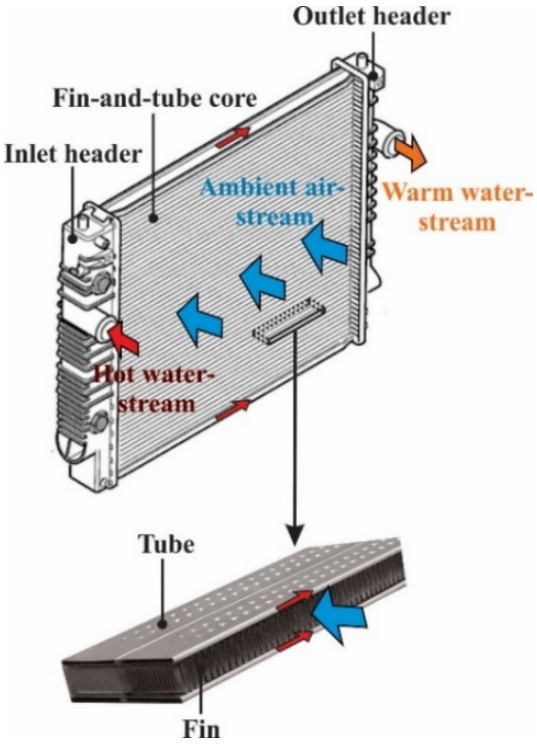


Figure 2. Heater core with hot coolant water flowing through its tubes and an ambient airstream impinging its surface.

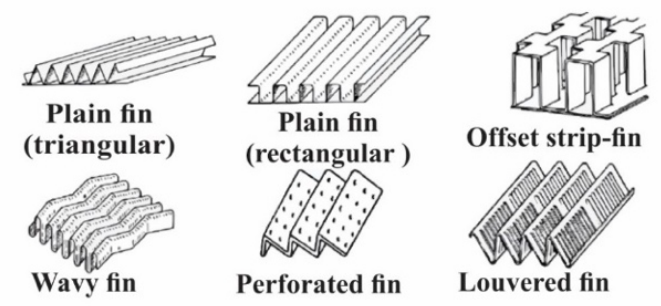
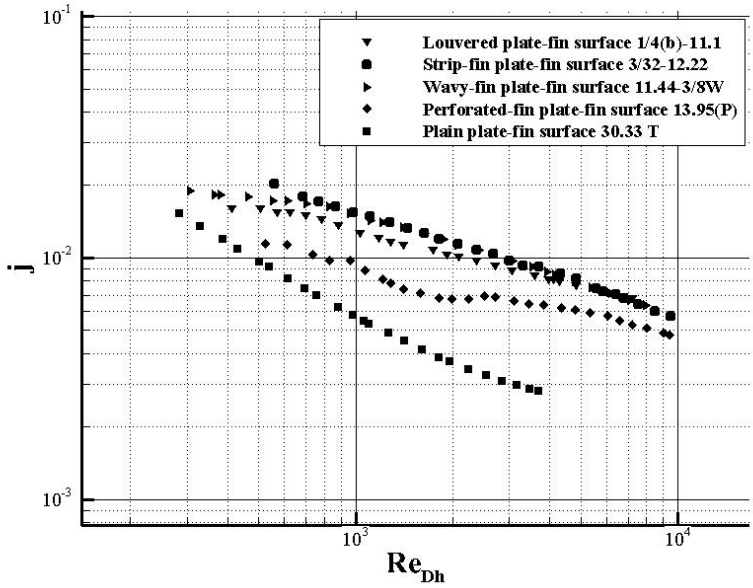
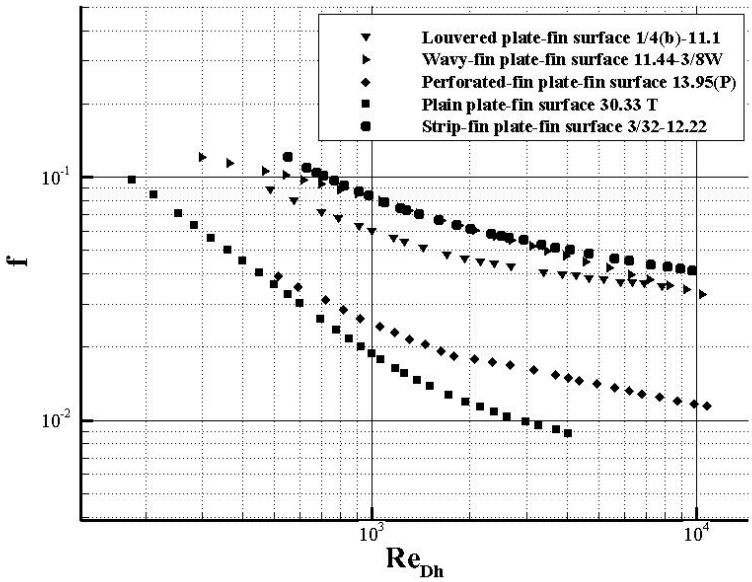


Figure 3. Common compact heat exchanger fin geometries [9].

Kays & London [3] and Jacobi & Shah [10] reported on the heat transfer and flow friction characteristics of several interrupted fins. Results (Fig. 4) showed that louvered fins, amongst other interrupted fins, provided a moderate heat transfer performance with relatively low pressure drop. This was owing to the fact that the flow resistance through louvered fins was mostly caused by skin friction drag, since the thin, flat, plate-like louvers had relatively small separated wakes downstream of the interruptions [11]. Due to low pumping power requirements for most ACCS units, louvered fins are a popular choice amongst heater core manufacturers in the automotive industry. Their thermo-fluidic nature has been studied in considerable engineering detail, for over 50 years, beginning with the first flow visualizations by Beauvais [12] who showed the existence of “louver-directed” flow, shown schematically in Fig. 5. Davenport [13] further emphasized that louver-directed flow was only prominent at high enough Reynolds numbers where the boundary layers over the louvers did not obstruct the louver passageways. Otherwise, a "duct-directed" flow would occur, in which the airstream would pass through the fins as if the louvers did not exist.



(a)



(b)

Figure 4. Performance data for plate-fin surface heat exchangers from Kays & London [3]: (a) Colburn j-factor vs Re, (b) friction factor vs Re.

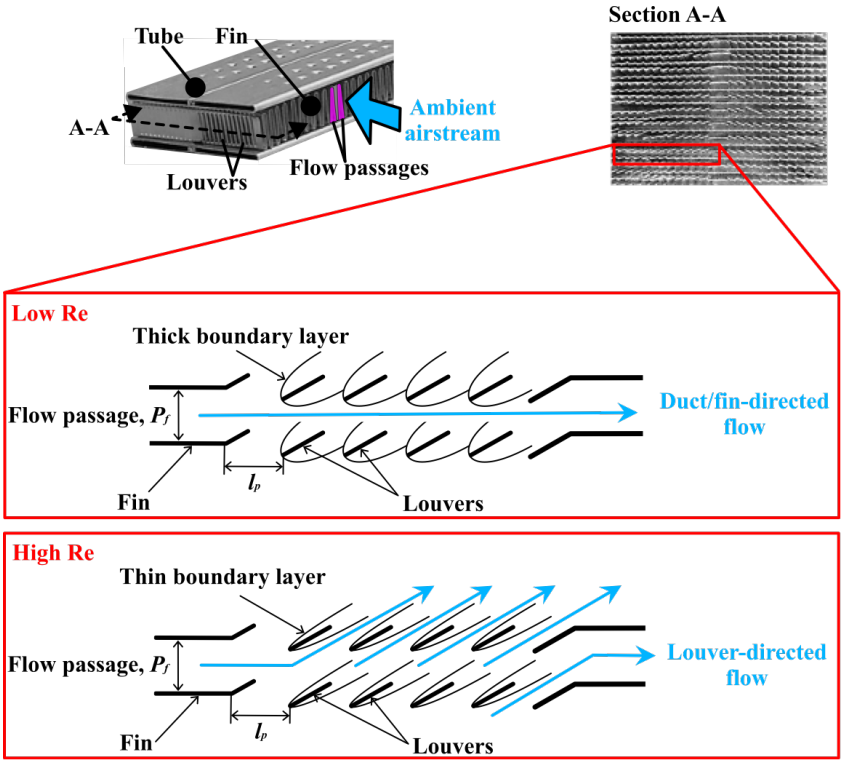


Figure 5. Airflow directions through louvered fins at low and high Reynolds numbers.

While louver-directed flow is preferred because it causes destruction of the thermal boundary layer and enhances heat transfer, it is not always possible, especially when the flow conditions upstream of the heater core are unfavourable. Experiments to characterize heater core performance (e.g., Fig. 4) are typically carried out under controlled conditions with uniform flow upstream of the core

impinging perpendicular to the core axis, no obstructions, and no duct area changes upstream and downstream of the core as shown in Fig. 6 (i.e., the “design conditions”). In practice, however, duct geometries and flow structures upstream of the heater core often deviate from the design conditions in one or more ways, giving rise to “off-design conditions”. For example, because the ACCS is a secondary vehicle component, minimization of the overall space consumed by the complete system beneath the hood is prioritized during its design. As a result, ACCS ducting contains tight turning angles for the airstream, as indicated in Fig. 7(a) by the circled region 1. As shown in Fig. 7(b), the flow area also increases from *h2* to *h3,* which decelerates the airstream and presumably aids flow separation behind the wedge-shaped obstruction. Thus, the airstream velocity profile incident on the heater core is likely to be non-uniform. Furthermore, the incidence angle is not expected to be parallel to the flow passage through the core (as is the case under design conditions), as shown in Fig. 7(a) by the circled region 2. With the ACCS's low pumping power availability, it is feasible that the heater core operates near or within the "low *Re*" region (Fig. 5), in which duct-directed flow would prevail anywhere there is a local flow deceleration (e.g., in a possibly separated wake behind the wedge). Therefore, off-design conditions should reduce the core’s thermal performance due to increased duct-directed airflow.

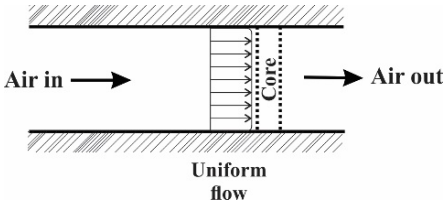


Figure 6. Schematic representation of the experimental setup used to characterize heater core performance at design conditions.

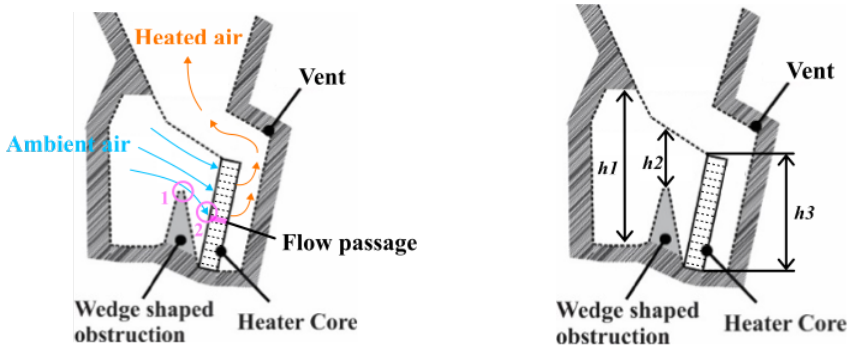


Figure 7. Geometry of an ACCS unit’s duct system showing the presence of off-design conditions in practice: (a) non-uniform and non-parallel incident airflow, (b) flow area changes upstream and downstream of the core.

Although louvered fin-and-tube cores offer favorable heat transfer and friction properties for use in automotive ACCS units, they suffer the aforesaid disadvantage of being sensitive to the flow

conditions upstream, and possibly also downstream, of the core. Few researchers, for example, [14-17], have demonstrated that non-uniform and non-parallel incident airstreams reduce the thermal performance of heater cores. These studies typically considered different off-design conditions in isolation, and frequently aimed to quantify the performance deterioration without specifically addressing the underlying physics in general. Previous studies have developed simulations, correlations, and frameworks to predict the performance of a louvered fin-and-tube core operating under a particular off-design condition. Importantly, however, the off-design conditions considered in the literature did not resemble those of typical ACCS units, such as that of Fig. 1(b). Indeed, ACCS unit performance data and internal duct geometries are rarely provided by manufacturers because they are proprietary technology. Hence, it is doubtful that the same performance data reported in the open literature applies to current and future ACCS units developed in the industry.

In this study, thermal performance data is obtained for a louvered fin-and-tube heater core operating under two off-design conditions typically encountered in a commercially manufactured ACCS unit as reference. In particular, these include an airflow obstruction upstream, and ducting downstream, of the heater core. The individual off-design conditions are considered systematically, both in combination and in isolation, with specific emphasis on the underlying physics responsible for the core's thermal performance reduction. By identifying and associating off-design performance deterioration with the underlying physics, logical steps proceed in the design of a new heater core which overcomes significant performance limitations imposed by off-design setups in commercial ACCS units. Thus, the current work shall fill a gap in the academic literature, i.e., specifically related to understanding the reasons why certain off-design conditions are harmful to louvered fin-and-tube performance. Through the new findings, the automotive industry also stands to gain from this work the development of a novel prototype heat exchanger to improve ACCS thermal performance.

1.2 Literature Review

1.2.1 Louvered fin-and-tube core operation at design conditions

Kays and London [3] were among the first to publish performance data (i.e., heat transfer and pressure drop data) for a myriad of extended surface heat exchangers. Most of the louvered surfaces considered did not geometrically conform to those used in modern automobile air-conditioning applications, yet the trend in their data set conforms to studies on automobile heat exchangers which later followed their experimental method.

Researchers initially believed that the flow through louvered fins was always duct-directed (i.e., the main flow did not follow the common louver angle), and that the louvers acted merely as a surface roughness which increased shear stress at the wall and therefore enhanced heat transfer. Beauvais [12], however, described a flow visualization technique (consisting of smoke flow injection, hot-wire anemometry and China-clay oil evaporation) which could prove that the louvers affected the

flow (particularly its direction) through the fins quite differently. Experimental data was only presented for a plain fin geometry, however, a single image of a smoke flow pattern through a louvered fin model was provided with no further details. According to Webb and Trauger [18], inspection of Beauvais' [12] image showed that (1) the louver angle was around $\theta = 30°$, (2) the ratio of louver pitch to fin pitch (denoted as l_p/P_f in Fig. 5) was close to 0.8, and (3) the main flow was parallel to the louvers for the velocities tested (i.e., the flow was actually louver-directed).

Davenport [13] presented steady-state experimental data for 8 louvered fin-and-tube cores in the range $300 \leq Re_{lp} \leq 1300$. It was seen that the slopes of the Stanton number (St) and friction factor (f) curves were similar to those of the laminar boundary layer solutions for heat transfer and skin friction drag over a flat plate, respectively, developed by Pohlhausen and Blasius [2]. This observation led to the idea that a similar mechanism (i.e., laminar boundary layer flow over a flat plate) could have been present in louvered fins, and the idea would confirm that the louvers did not behave merely as a surface roughness with duct-directed flow through the fin passage, but instead behaved as an array of flat plates directing the flow along the common louver angle.

According to Achaichia & Cowell [19], Davenport's work suggested that, for sufficiently high Reynolds numbers (i.e., $Re_{lp} > 300$), the effect of louvers was to align the flow parallel to the louver plane (i.e., to promote the louver-directed flow shown in Fig. 5), which is consistent with the smoke-flow trace provided by Beauvais [12]. In addition, the degree of alignment of the flow with the louvers reduced significantly as the Reynolds number decreased, resulting in "flattening" of the Stanton number (St) curve at very low Re_{lp} (i.e., below $Re_{lp} \approx 100$), as shown in Fig. 8. Flattening (or gradient changes in general) of the log-scale St versus Re_{lp} curve (where St is defined as the ratio between Nu_{lp} and $Re_{lp} \cdot Pr$) suggests a change in the power-law relationship between Nu and Re_{lp}. Therefore, there must have been a corresponding change in the fluidic nature of the mechanism driving heat transfer, for flattening to occur. This was taken as indication of some "transition" between distinct flow structures inside the louver array, which occurred as Re_{lp} was gradually reduced. Achaichia & Cowell's experimental work showed that curve flattening commenced at various Re_{lp} depending on the core geometry. In particular, for samples with low values of l_p/P_f and louver angle, θ, curve flattening was observed at approximately $Re_{lp} = 1000$, while for other samples it was only observed for $Re_{lp} < 600$. Their data clearly showed similarity with the Pohlhausen curve, in line with Davenport's observation. As the Reynolds number was reduced further, below the curve flattening region, the data points seemed to match the solution to laminar internal flow through a duct, albeit very roughly with just a few data points in that region. Thus, it was reasoned by the authors that curve flattening indicated a transition from flat-plate flow (which could have only occurred if the flow was louver-directed) to duct flow (which could have only occurred if the flow was duct-directed).

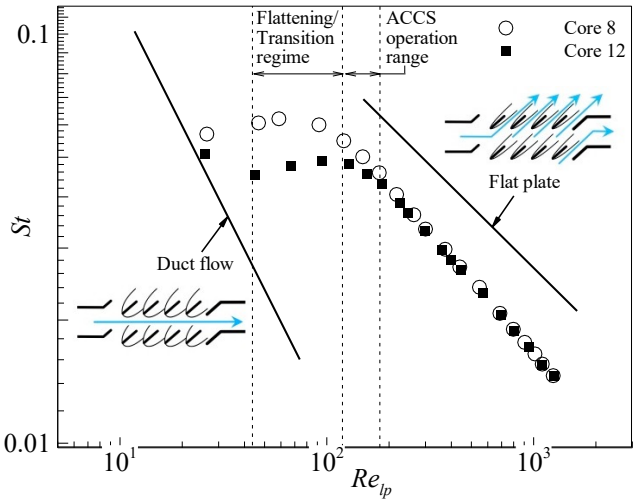


Figure 8. Flattening of the Stanton number curve, indicating transition from duct flow to flat-plate flow, in two representative louvered fin-and-tube cores studied by Achaichia & Cowell [19].

Although Achaichia & Cowell's observation confirmed the existence of two distinct flow structures in the different Reynolds number regimes, the dependence of the transition on Re_{lp}, l_p/P_f, and θ was not clear. Webb & Trauger [18] carried out detailed flow visualization studies on 10:1 scale louvered fin models, to characterize the variation of the "flow efficiency" (i.e., the extent of louver-directed flow) with increasing Reynolds number Re_{lp}, louver pitch to fin pitch ratio l_p/P_f, and louver angle θ. For all l_p/P_f the flow efficiency increased with Re_{lp}, until a critical Reynolds number Re_{lp}^* was reached. Thereafter, the flow efficiency became independent of both Re_{lp} and θ. Increase of the louver angle from $\theta = 20°$ to $\theta = 30°$ resulted in increased flow efficiency only for $Re_{lp} < Re_{lp}^*$, and a slight decrease of the critical Reynolds number, from Re_{lp}^*=1380 to Re_{lp}^*=1200. Flow efficiency also increased with l_p/P_f, and the flow efficiency was maximum (i.e., 100% louver-directed) only for $l_p/P_f > 1.31$. These findings were generally consistent with later researchers [20, 21].

Several correlations detailing the thermo-fluidic performance of louvered fin-and-tube heater cores have since been reported in open literature [3, 13, 19, 22-25], for heater core operation under design conditions, most notably by Chang & Wang [22] whose correlation was derived from the largest single data set to date. It is generally understood that increased heat transfer and pressure drop are associated with increased louver-directed flow. For a louver-directed flow system to be prevalent, it is firstly required that the geometry of the louvered fin (e.g., the ratio of louver pitch to fin pitch l_p/P_f) minimizes hydraulic resistance in the preferred (louver-directed) path [18, 20]. Additionally, maintaining louver-directed flow requires a sufficiently large Reynolds number to preserve thin hydrodynamic boundary layers at louver entrances, which avoids blockage of fresh main-stream flow from entering the louver passages. These requirements are reflected in the correlations shown in Table 1, where the magnitudes of the exponents indicate the sensitivities of the heat transfer coefficient (expressed in terms of the Colburn j-factor) and the friction factor, f, to the respective

geometrical parameters of the fin, as well as the Reynolds number. For example, researchers have determined strong sensitivities to the louver angle, θ, whereas weaker sensitivities to the fin thickness, δ, were consistently reported.

Table 1. Published heat transfer and friction factor correlations

Authors	**Correlation**	**Precision**	**Valid Range**
Achaichia & Cowell (1988) [19]	$St = 1.554\frac{\left(0.936 - \frac{243}{Re_{lp}} - 1.76\frac{P_f}{l_p} + 0.995\theta\right)}{\theta} Re_{lp}^{-0.59}\left(\frac{P_t}{l_p}\right)^{-0.09}\left(\frac{P_f}{l_p}\right)^{-0.04}$	98% of data within $\pm 10\%$	$Re_{l_p} > 75$
	$f = 0.895 f_A^{1.07} P_f^{-0.22} l_p^{0.25} P_t^{0.26} l_h^{0.33}$ where $f_A = 596 Re_{l_p}^{0.318 log Re_{lp}^{-2.25}}$		$150 \leq Re_{l_p} \leq 3000$
	$f = 10.4 Re_{l_p}^{-1.17} P_f^{0.05} l_p^{1.24} P_t^{0.83} l_h^{0.25}$	91% of data within $\pm 10\%$	$Re_{l_p} < 150$
Chang & Wang (1997) [22]	$j = Re_{l_p}^{-0.49}\left(\frac{\theta}{90}\right)^{0.27}\left(\frac{P_f}{l_p}\right)^{-0.14}\left(\frac{b}{l_p}\right)^{-0.29}\left(\frac{L_t}{l_p}\right)^{-0.23}\left(\frac{l_l}{l_p}\right)^{0.68}\left(\frac{P_t}{l_p}\right)^{-0.28}\left(\frac{\delta}{l_p}\right)^{-0.05}$	89. 3% of data within $\pm 15\%$	$100 < Re_{l_p} < 3000$
Kim & Bullard (2002) [23]	$j = Re_{l_p}^{-0.487}\left(\frac{\theta}{90}\right)^{0.257}\left(\frac{P_f}{l_p}\right)^{-0.13}\left(\frac{b}{l_p}\right)^{-0.29}\left(\frac{L_f}{l_p}\right)^{-0.235}\left(\frac{l_l}{l_p}\right)^{0.68}\left(\frac{P_t}{l_p}\right)^{-0.279}\left(\frac{\delta}{l_p}\right)^{-0.05}$	Rms error $\pm 14.5\%$	$100 < Re_{l_p} < 600$
	$f = Re_{l_p}^{-0.781}\left(\frac{\theta}{90}\right)^{0.444}\left(\frac{P_f}{l_p}\right)^{-1.682}\left(\frac{b}{l_p}\right)^{-1.22}\left(\frac{L_f}{l_p}\right)^{0.818}\left(\frac{l_l}{l_p}\right)^{1.97}$	Rms error $\pm 7\%$	$100 < Re_{l_p} < 600$
Dong et al. (2007) [24]	$j = 0.26712 Re_{l_p}^{-0.1944}\left(\frac{\theta}{90}\right)^{0.257}\left(\frac{P_f}{l_p}\right)^{-0.5177}\left(\frac{b}{l_p}\right)^{-1.9045}\left(\frac{l_l}{l_p}\right)^{1.7159}\left(\frac{L_f}{l_p}\right)^{-0.2147}\left(\frac{\delta}{l_p}\right)^{-0.05}$	95% of data within $\pm$ 10%	$250 < Re_{l_p} < 2500$
	$f = 0.54486 Re_{l_p}^{-0.3068}\left(\frac{\theta}{90}\right)^{0.444}\left(\frac{P_f}{l_p}\right)^{-0.9925}\left(\frac{b}{l_p}\right)^{0.5458}\left(\frac{L_f}{l_p}\right)^{0.0688}\left(\frac{l_l}{l_p}\right)^{-0.2003}$	95% of data within $\pm 12\%$	$250 < Re_{l_p} < 2500$

Shinde & Lin (2017) [25]	$j = Re_{l_p}^{-0.324}\left(\frac{P_f}{l_p}\right)^{-0.2}\left(\frac{b}{l_p}\right)^{-2.3}\left(\frac{\delta}{l_p}\right)^{-0.001}\left(\frac{\theta}{90}\right)^{1.1}\left(\frac{l_l}{l_p}\right)^{1.72}\left(\frac{H_t}{l_p}\right)^{1.88}\left(\frac{L_f}{l_p}\right)^{-0.195}$	85.3% of data within ±19.68%	$20 < Re_{l_p} \leq 80$
	$j = Re_{l_p}^{-0.4}\left(\frac{P_f}{l_p}\right)^{-0.07}\left(\frac{b}{l_p}\right)^{-2.48}\left(\frac{\delta}{l_p}\right)^{-0.006}\left(\frac{\theta}{90}\right)^{0.09}\left(\frac{l_l}{l_p}\right)^{1.83}\left(\frac{H_t}{l_p}\right)^{1.65}\left(\frac{L_f}{l_p}\right)^{-0.012}$	84.8 % of data within ± 22.12%	$80 < Re_{l_p} \leq 200$
	$f = Re_{l_p}^{-0.87}\left(\frac{P_f}{l_p}\right)^{-0.06}\left(\frac{b}{l_p}\right)^{-0.014}\left(\frac{\delta}{l_p}\right)^{-1.35}\left(\frac{\theta}{90}\right)^{0.67}\left(\frac{l_l}{l_p}\right)^{0.007}\left(\frac{H_t}{l_p}\right)^{0.83}\left(\frac{L_f}{l_p}\right)^{0.019}$	85.3% of data within ± 13.53%	$20 < Re_{l_p} \leq 80$
	$f = Re_{l_p}^{-0.856}\left(\frac{P_f}{l_p}\right)^{-0.016}\left(\frac{b}{l_p}\right)^{-0.01}\left(\frac{\delta}{l_p}\right)^{-1.1121}\left(\frac{\theta}{90}\right)^{0.74}\left(\frac{l_l}{l_p}\right)^{0.31}\left(\frac{H_t}{l_p}\right)^{0.53}\left(\frac{L_f}{l_p}\right)^{0.053}$	85.6% of data within ±10.68%	$80 < Re_{l_p} \leq 200$

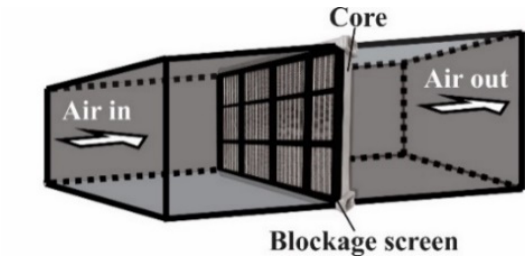
The foregoing correlations apply for large Reynolds numbers (i.e, typically $Re_{lp} > 100$) wherein the flow is characterized as laminar and increasing unsteadiness (i.e., consisting of recirculating regions, either at the leading or trailing edges of the louvers, or both) with Re_{lp}, throughout the louver array [21, 26]. At lower Reynolds numbers ($Re_{lp} < 100$), curve flattening was usually not accounted for and unsteadiness in the louver array was due only to recirculation in the wake of all louvers [21, 25, 26]. The correlation proposed by Achaichia & Cowell [19] includes a subtle adjustment to reflect curve flattening, but researchers have inconsistently reported the exact Reynold's number at which it initially occurs. Shinde & Lin [25] aimed to clarify this behaviour, noting that most previous studies had only a few data points in the low Reynolds number range $Re_{lp} < 100$. The authors characterized the heat transfer and pressure drop performance of twenty-six commercially available heat exchangers with various fin pitch P_f, fin height l_h, fin thickness δ, louver pitch l_p, louver angle θ, louver length l_l, tube height H_t, and flow depth L_t in the range $20 \leq Re_{lp} \leq 200$, and observed flattening behaviour of the j-factor curve in at least half of their samples, to a greater or lesser extent depending on the sample geometry, leading to a discontinuous correlation: one for low Reynolds numbers and another for higher Reynolds numbers as shown in Table 1. The cause for flattening occurring at different Reynolds numbers was not explicitly stated, and it was not made clear why only 50% of their samples showed the phenomenon. Nonetheless, the development of separate correlations by Shinde and Lin indicated consistency with the observations of Davenport [13], Achaichia & Cowell [19], Webb & Trauger [18], and others [12, 20, 24, 27], that distinct flow structures (i.e., duct- and louver-directed flow) occur at low and high Reynolds number regimes, with a transition in-between.

1.2.2 Performance deterioration at off-design conditions

Although the thermo-fluidic performance of louvered-fins is generally established for design conditions at a reasonably high Reynolds number, various off-design conditions are encountered in

typical air-conditioning systems, including ACCS units, mainly due to space constraints during their integration into their larger systems. The heater core positioned in a typical ACCS unit is shown schematically in Fig. 7 where the geometrical features inside the unit substantially deviate from the design setup of Fig. 6. Upstream of the heater core is a wedge obstruction to the flow, and downstream of the core is a vertically oriented duct. As a result, the assumption of design conditions characterized by previous correlations are not expected to be valid when making performance predictions for the heater core operating inside an ACCS unit.

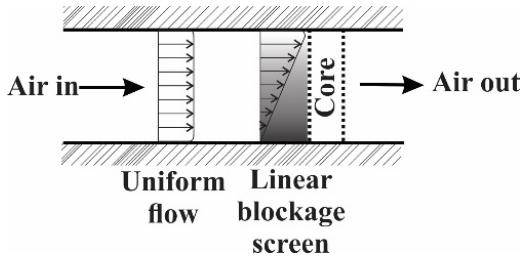
Airflow non-uniformity at the inlet of the heater core, caused by compact ducting, is a common off-design condition encountered in typical air-conditioning systems [28]. The effects of various inlet air-flow distributions on the thermal performance of louvered fin-and-tube cores have usually been studied by blocking the airflow path through the core with a blockage screen, as shown in Figs. 9(a,b), which results in a non-uniform velocity profile upstream of the core (Fig. 9(c)). T'Joen et al. [14] found that linear and quadratic velocity distributions resulted in 8.2% and 3.4% reductions in the overall heat transfer coefficient, respectively. Datta et al. [15] considered four types of blockages upstream a louvered fin-and-tube condenser core and concluded that the side blockage resulted in the most severe (up to 8.16%) reduction in cooling capacity. Blecich [16] found up to 30% reduction in thermal performance when extremely non-uniform airstream velocity profiles were incident on the core, and 5-10% thermal performance reduction when moderate non-uniformities were encountered. While the foregoing studies have shown thermal performance degradation due to air-flow non-uniformity, the artificially created velocity profiles were typically one-dimensional (i.e., non-uniformity was introduced in a single velocity component). In addition, off-design conditions downstream of the core were not studied and the bulk flow typically remained perpendicular to the core axis. Due to space limitations, two cores can also be arranged with an "A" (or "V") configuration, or a single core can be inclined (at a non-perpendicular angle) relative to a uniform airstream as shown in Fig. 9(d). Core inclination within the uniform flow field has been shown to be insignificant for airstream velocities between 0.6 - 2 m/s, by Kim et al. [17] who inclined a full-scale core to a maximum of 60^{o}. At higher airstream velocities (i.e., between 1.9 – 9.8 m/s), however, Henriksson [29] reported a 36% heat transfer enhancement at 60^{o} inclination.



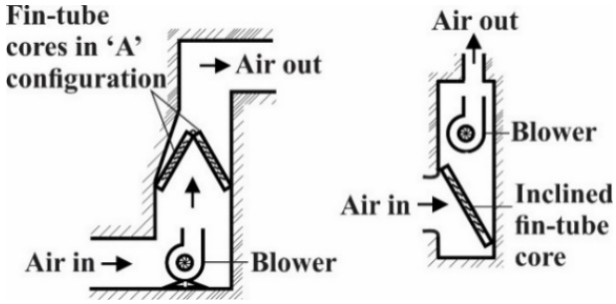
(a)



(b)



(c)



(d)

Figure 9. Typical off-design conditions previously studied: (a) blockage screen position upstream of a core, (b) blockage screens studied by Datta et al. [15] and Blecich [16], (c) effect of a linear blockage screen on the velocity profile of an incident airstream, (d) common configurations with "A" type and inclined fin-and-tube cores in central air-conditioning systems.

The foregoing studies indicated a clear dependence of the louvered fin-and-tube core's heat transfer performance on the flow conditions upstream of the core. Researchers developed models for predicting the performance of the cores with varying severity of individual off-design conditions, and concluded that performance was typically affected more as the severity increased. In an ACCS unit, several off-design conditions are present including inclination, non-uniform incident flow, and downstream ducting. However, it is not clear from the literature whether the performance models developed for isolated off-design conditions can be superimposed to produce a prediction for a combination of off-design conditions existing simultaneously. This study will consider off-design conditions both in isolation and in combination, primarily to understand the underlying fluidic mechanisms causing the thermal performance deterioration. In doing so, the validity of superimposing previous models to predict performance will be clarified.

1.2.3 Preventing off-design performance deterioration with aerodynamic anisotropy

Blecich [16] alluded to favourable orientations between the air velocity gradient and the fin plane, reporting that the degree of air redistribution by a straight finned core contributed to its overall thermal performance. The author mentioned that the redistribution characteristics of a core may, in turn, be affected by fin interruptions such as slits or louvers, but this was not explicitly quantified. With only two possible flow paths through a typical louvered fin (i.e., duct- or louver-directed), a louvered fin-and-tube core has been shown to have limited ability to disperse (i.e., to spread out, or re-distribute) an incidentally non-uniform airstream. In this connection, flow visualization studies [18, 20, 27] suggest that a streamline from an inlet deflection louver proceeds to the corresponding exit louver (on the same fin), regardless of whether the flow is duct- or louver-directed, as shown in Fig. 10. Here, there is no lateral dispersion of the airflow through the core and the airflow follows the shortest possible distance. This limitation should decrease the heat transfer capability of the core when operated under non-uniform airstreams, because a portion of the core's surface area would not be accessible to air with a high enough local Reynolds number to sustain louver-directed flow.

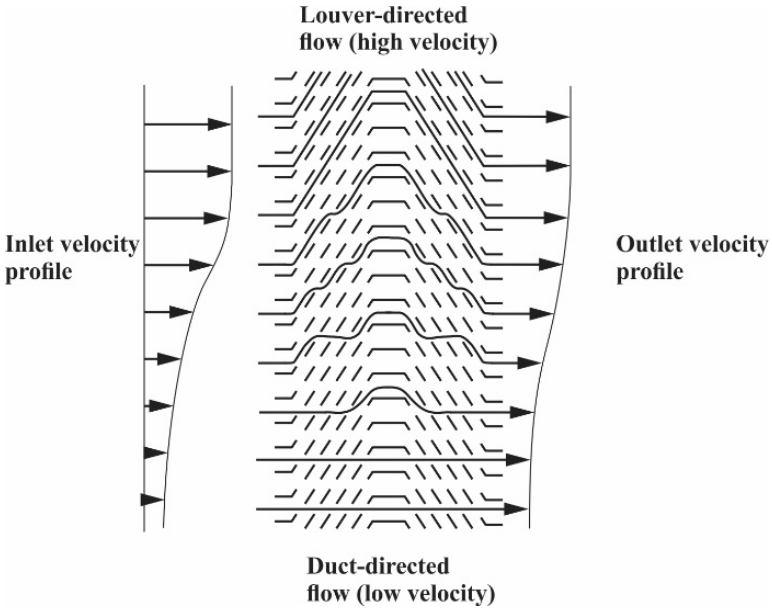


Figure 10. Typical flow paths and exit velocity profile for louvered fins with non-uniform incident velocity profile (adopted from Bellows [27]).

Due to their inherent inability to disperse an airstream, the overall heat transfer performance of louvered fin-and-tube cores is thought to be sensitive to local distortions in the inlet velocity distribution. However, to the best of the author's knowledge, no systematic evidence confirming this conjecture has previously been provided.

Flow maldistributions can typically be overcome with specially designed intakes or headers which disperse fluid momentum before entering a fluidic device. For example, Barratt & Kim [30] developed a wide-angle diffuser with an optimized cylinder bank within it to promote uniform

airflow at a diffuser exit, just before the airstream entered an electrostatic preciptator. For the same purpose (i.e., to promote uniform airflow), Kusuda et al. [31] proposed special manifolds designed for the intakes of a novel aviation heat exchanger. However, for compact units such as an ACCS, there is rarely extra space for additional components. Since off-design conditions upstream of the core are often unavoidable, ACCS unit performance must be increased by replacing louvered fin-and-tube cores with a core whose performance is fully exploited at off-design conditions.

Based on the literature, overcoming thermal performance losses at off-design conditions requires that the core is firstly insensitive to the incoming airstream's velocity profile. Thus, the core's external heat transfer surfaces must maintain the same dominant heat transfer mechanism over a wide range of Reynolds numbers and should be geometrically isotropic to provide insensitivity to the flow direction as well. Furthermore, to ensure that no portion of the core is short of sufficient coolant flux upon encountering a non-uniform incident airstream, hydraulic dispersion (i.e., re-distribution of fluid momentum) of the non-uniform airstream must occur during its passage through the heater core. Developing and testing a heater core with hydraulic dispersion capability should also provide insight into the reason why louvered fin-and-tube cores are sensitive to flow non-uniformity.

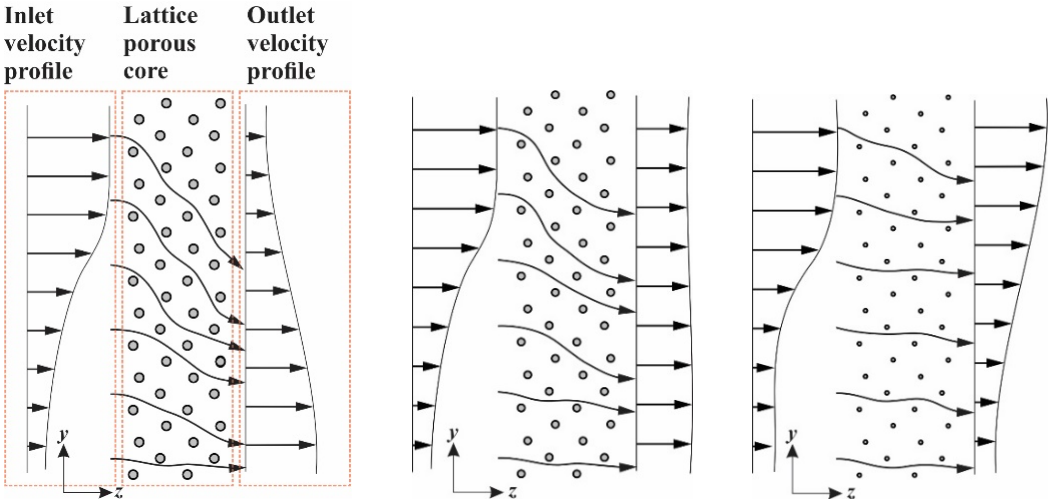


Figure 11. Flow paths and velocity profiles for porous media with non-uniform incident velocities (adopted from Barratt & Kim [32]): (a) Low porosity & high lateral dispersion, (b) Critical porosity, (c) High porosity & low lateral dispersion.

Hydraulic dispersion will occur if the static pressure gradient across the core is engineered, such that local streamlines having different kinetic energies are guided through the core in different directions. In this context, consider cylindrical extended surfaces which have been shown to have aerodynamic anisotropy (i.e., directional dependence of the level of drag experienced by the incident stream) when arranged in a staggered bank [33]. Barratt & Kim [32] leveraged this property of staggered cylinder banks to prevent a non-uniform velocity profile at the exit of a wide-angled diffuser. In

their case, high momentum fluid flowing longitudinally was redirected laterally when flowing through the cylinder bank, because the bank had a larger drag coefficient in the longitudinal direction; low momentum fluid naturally experienced relatively less lateral redirection. Importantly, Barratt & Kim's results proved that aerodynamic anisotropy could be altered by simply changing the bank's porosity. Based this idea, a similar construction is considered for the heater core in this study to disperse any non-uniform flows incident on the core. That is, by altering the bank's porosity as illustrated in Fig. 11, the heater core's relative drag coefficients in the longitudinal (z) and lateral (y) directions can be tailored to direct flow laterally through the heater core. When lateral dispersion occurs optimally within the core (i.e., at the "critical porosity"), regions of concentrated momentum in the incident flow field will be redirected, causing equal exposure of all parts of the core to the incident airstream. This will be indicated by a uniform velocity profile downstream of the core, as shown in Fig. 11(b).

1.3 Research Objectives and Methods

Individual off-design conditions have been investigated previously. Each off-design condition affects the thermal performance of a louvered fin-and-tube heater core to a greater or lesser extent. However, to the best of the author's knowledge, there has been no systematic study describing the performance of louvered fin-and-tube heater cores under a combination of off-design conditions, even though they are expected inside a commercial ACCS unit.

This study firstly characterizes the differences in thermal performance between a louvered fin-and-tube heater core operating inside (1) a uniform external airstream (i.e., at design conditions) and (2) a commercially manufactured ACCS unit (i.e., at a combination of off-design conditions). Thereafter, systematic fluidic and temperature measurements are carried out using purpose-built wind-tunnels, which are adjusted progressively to mimic conditions inside the ACCS unit. Using this technique, the contributions of each individual off-design condition to the overall thermal performance deterioration of the core will be ascertained. Further flow measurement and visualization will be carried out to gain insights into possible fluidic mechanisms responsible for the deterioration.

To demonstrate the validity of proposed fluidic mechanisms, and to prove that thermal performance deterioration due to off-design conditions can be overcome practically by introducing suitable aerodynamic anisotropy, a new heater core (i.e., a "lattice porous" heater core) will be developed to improve ACCS thermal performance. The lattice porous core shall feature specially arranged longitudinal and transverse circular ligaments that function, respectively, as tubes for hot water to flow internally through the core, and as solid cylindrical fins to promote aerodynamic anisotropy and enhance convection to the external airstream.

The lattice porous core's ability to redistribute a non-uniform incident airstream will be assessed, by time-averaged airflow measurements, to find the fin diameter required for critical porosity (Fig. 11(b)). Once found, the heat transfer performance of the lattice-porous core will be compared to that of a conventional louvered fin-tube core under both uniform and non-uniform incident airstreams. The contribution of circular fin ligaments, to the overall heat transfer performance of the lattice porous core, will also be discussed explaining the role of thermal dispersion in improving thermal performance of heater cores under off-design conditions.

1.4 Publications

This dissertation is based on the following publications, for which the author was responsible for the problem formulation, experimental setup, data collection, manuscript authorship, submission to the journal, and manuscript revisions based on peer-reviewed feedback:

1. **T.I. Bhaiyat**, S.W. Schekman, H.Y. Lim, Y.H. Jeon, T. Kim (2019), "Off-design performance of a louvered fin-tube heater core in an automotive climate control system," *Applied Thermal Engineering* 161: 114155. https://doi.org/10.1016/j.applthermaleng.2019.114155
2. **T.I. Bhaiyat**, T.J. Lu, T. Kim (2020), "Lateral diffusion in a lattice porous heater core for compact operations," *Applied Thermal Engineering* 176: 115430. https://doi.org/10.1016/j.applthermaleng.2020.115430

2 EXPERIMENTS

This study primarily seeks experimental measurement of the thermo-fluidic performance of two different heater cores, namely (1) a conventional louvered fin-and-tube heater core, and (2) a newly designed "lattice porous" heater core. Comparison of both cores' thermal performance and fluidic behaviour under design conditions (Fig. 6), and under off-design conditions (Fig. 7), is sought. Thus, the following sections detail the methods, apparatus, and test rigs built to obtain and process the relevant heat transfer and hydraulic data. The experimental setups used to obtain data are described first, followed by: a description of the two heater core geometries, the data reduction method and an uncertainty analysis.

2.1 Test Rig and Setups

In this section, a water heating circuit used to simulate hot engine coolant for all of the cores tested is first described. Next, the construction of wind tunnels used to collect data for each core under design-conditions is detailed. A commercial ACCS unit (representing a combination of off-design conditions) in which the louvered fin-and-tube core's thermal performance was measured is also described. Details of modifications made to the wind tunnels, in order to incrementally match the ACCS unit's off-design conditions (i.e., simulated off-design conditions) are then provided, followed by a description of time-averaged thermal and fluidic measurement techniques used in each test. Finally, flow visualization and temperature mapping methods, used to provide further insights into the fluid flow and heat transfer data are described.

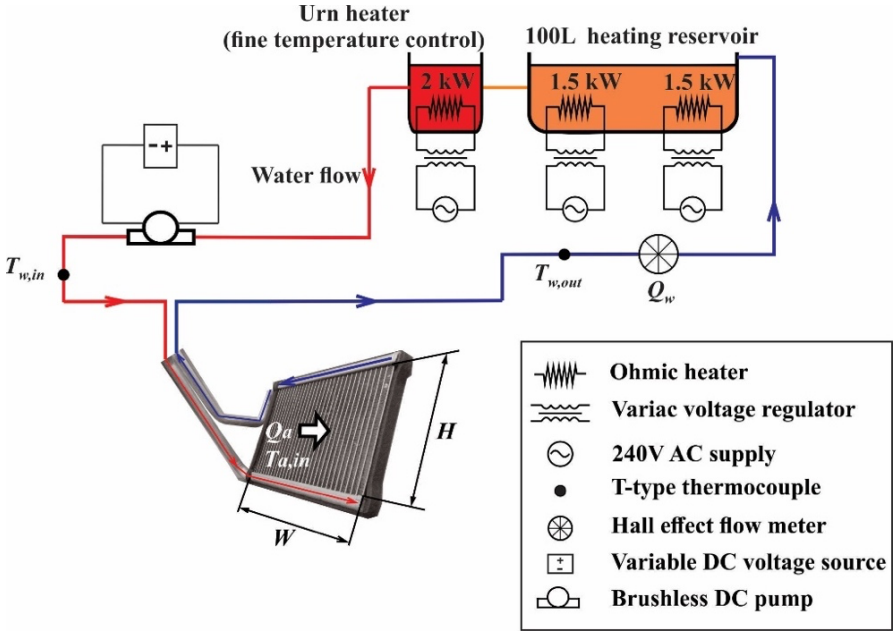
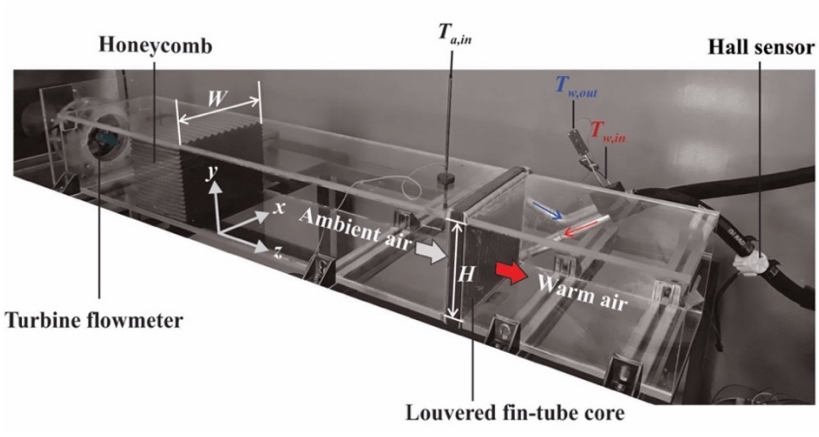


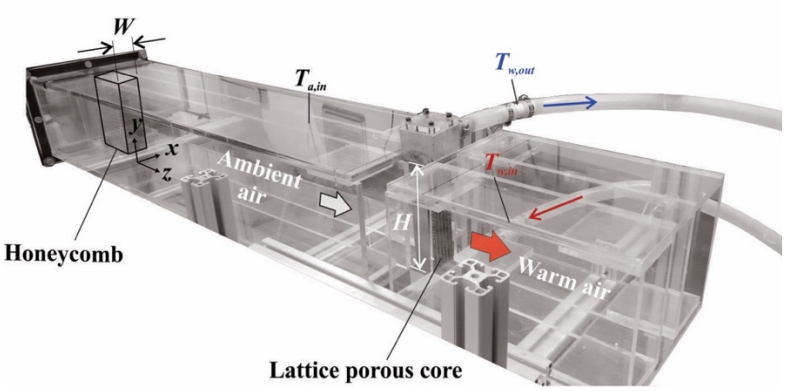
Figure 12. Schematic of hot water supply and measurement system for waterflow through the header tubes of a test core.

2.1.1 Water heating circuit

To measure the thermal performance of a heater core, the core was first furnished with a closed-loop hot water supply system, shown schematically in Fig. 12, before being placed inside the test section of one of the custom-built wind-tunnels (Fig. 13). A 12 V brushless DC pump circulated water, through a series of electrical heaters before passing through the core, at a constant volume flowrate of Q_w = 0.11925 *L/s*. Each electrical heater (with maximum power rating indicated in Fig. 12) was connected to an independent voltage regulator to adjust the electrical power input.



(a)



(b)

Figure 13. Blowdown rectangular wind-tunnel showing the transverse (*x*), lateral (*y*), and longitudinal (*z*) directions for: (a) a louvered fin-and-tube heater core positioned in the test section, (b) a lattice porous heater core positioned in the test section.

T-type thermocouples were placed at 4.5L_t upstream of the inlet header, and at 4.5L_t downstream of the outlet header, to measure the core's inlet and outlet water temperatures, $T_{w,in}$, and $T_{w,out}$, respectively.

Similar to the method adopted by Shinde [34], the 2 kW urn heater was installed to provide a backup heating system during testing, and to minimize variations of the inlet water temperature. Using this

approach, the experimental setup was capable of temperature variations less than 0.5 °C within the range of air volume flowrates used in this study (i.e., $0 \leq Q_a \leq 160$ *L/s*).

2.1.2 Design performance test setup

For thermal performance characterization at design conditions (Fig. 6), a heater core connected to the hot water supply system was placed inside the test section of a wind tunnel that provided a uniform airstream upstream of the core, as shown in Fig. 13(a).

A 0.9 kW centrifugal fan capable of providing volume flowrates in the range $0 \leq Q_a \leq 200$ *L/s* blew air at ambient temperature through a circular tube that was fitted with a turbine flowmeter from Airflow™, UK (LCA501). Downstream of which, a long rectangular flow developing section (having variable width, 47.6 mm < W < 225 mm and constant height, H = 160 mm) with its length of 10 times the turbine's rotor diameter (d), was attached. Inside the channel, a honeycomb layer was positioned at 2d downstream from the inlet of the flow developing section. At the outlet side of a heater core, another short rectangular channel was placed to avoid a sudden expansion of the airstream that leaves the core. Since the lattice porous core had a smaller width than the louvered fin-and-tube core, the test-section cross-sectional width (W) was reduced by inserting acrylic plates upstream and downstream of the test section as shown in Fig. 13(b).

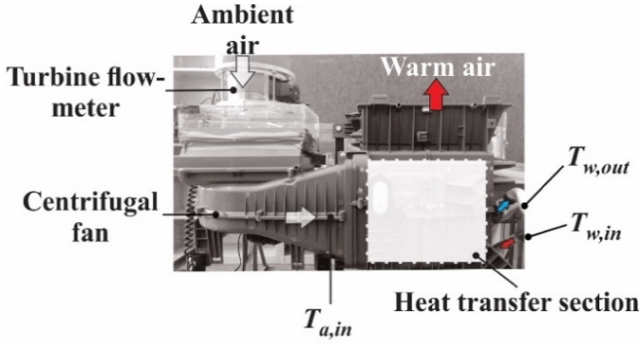
A T-type thermocouple was placed at the mid-height of the wind tunnel (i.e., 0.5H) and 4 times the tube depth (i.e., 4L_t) upstream of the test-section to measure the temperature of the airstream ($T_{a,in}$) before it passed through the core.

To measure turbulence intensity inside the wind-tunnel, a hot-wire anemometer (a straight single-sensor probe, 55P11, Dantec Inc.) of thickness 5 μm was positioned at the mid-channel height and width and 4 times tube depth (i.e., 4L_t) upstream, acquiring signals at a sampling frequency of 10 kHz for a duration of 3.3 seconds. Calibration was performed by the probe against a Pitot tube in the main-stream. The turbulence intensity was measured to be 2.5% at an air-side Reynolds number of Re_{lp} = 200.

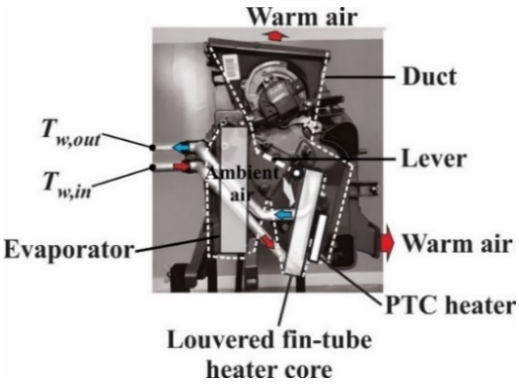
2.1.3 Off-design performance (ACCS unit) test setup

For off-design thermal performance characterization, a louvered fin-and-tube heater core furnished with the hot water supply system was placed inside a complete ACCS unit, as shown in Fig. 14. The unit's centrifugal fan drew air from the surroundings and blew it, through a diffuser, towards a heat transfer section containing louvered fin-and-tube evaporator and heater cores. Inside the heat transfer section, air flows through the heater core as shown schematically in Fig. 7(a).

A T-type thermocouple was placed in-between the outlet of the centrifugal fan and the heat transfer section, to measure the temperature of ambient air, $T_{a,in}$, entering the heater core.



(a)



(b)

Figure 14. Automotive climate control system (ACCS) unit used in this study to characterize the combined off-design conditions typically found in automobile air-conditioning systems: (a) Frontal view, (b) Side view.

2.1.4 Simulated off-design performance test setups

To investigate off-design conditions, the original test sections (Fig. 13) were modified to replicate flow conditions inside the ACCS unit. Thus, two primary modifications were made. Firstly, a right-angled wedge-shaped obstruction (with base $1.85L_t$, height $0.625H$, and depth W) was placed upstream of the core (Fig. 15(a)) to promote a non-uniform incident airstream. Secondly, ducting was included downstream of the core (Fig. 15(b)) to promote a sharp redirection of the airstream.

In the first configuration, the wedge was inserted immediately upstream of the heater core. Downstream of which, there were no further obstructions (Fig. 15(a)). This configuration showed the effect of the wedge in isolation, representing what is referred to in this study as “half-ACCS unit” conditions.

In the second configuration, a plate was inserted downstream of the core, which closed off the airflow path behind it. Air vents drilled into the wind tunnel ceiling directed the airstream upward, as shown schematically in Fig. 15(b). This configuration showed the effect of downstream ducting on half-ACCS unit conditions, representing what is referred to in this study as “full-ACCS unit” conditions.

Other flow area contractions or expansions, as well as airstream inclinations, upstream of the heater core, were understood to have negligible effects on the core's thermal performance [17, 29] within the range of practical ACCS flowrates, and were therefore not considered in this study.

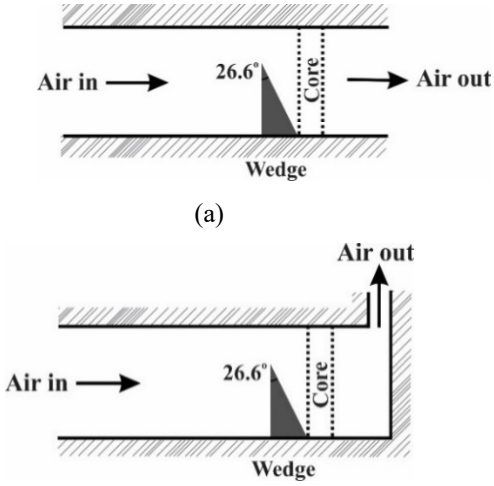


Figure 15. Schematic representation of wind tunnel modifications used in this study to simulate individual and combined off-design conditions found in the ACCS unit: (a) A wedge obstruction placed immediately upstream of the heater core and no downstream ducting (i.e., half-ACCS unit), (b) An upstream wedge obstruction and upward ducting downstream of the heater core (i.e., full-ACCS unit).

2.1.5 Temperature measurements

For each core, having hot water fed through at a constant water-side Reynolds number $Re_w \approx 1000$ (based on the tube's internal hydraulic diameter) and constant water inlet temperature $T_{w,in} = 55$ °C, the exit temperature of the water-stream, $T_{w,out}$, and the inlet temperature of the airstream, $T_{a,in}$, were recorded at steady-state, for several airstream flowrates varying systematically in the range $30 < Q_a < 90$ L/s. All thermocouple signals ($T_{a,in}$, $T_{w,in}$, and $T_{w,out}$) were recorded at steady-state by a Keysight 34972A data acquisition system.

2.1.6 Airstream flowrate and velocity profile measurements

To measure the volume flowrate of an airstream, Q_a, flowing through the ACCS unit, a pre-calibrated digital rotating vane anemometer from Airflow™, UK (LCA501) was mounted on the intake the ACCS unit (as shown in Fig.14(a)). There was a fabric filter between the rotating vane anemometer and the fan inlet as a default setup in the ACCS unit. The centrifugal fan was connected to a DC power supply unit (RPE-4323) capable of providing a variable output voltage and current, between 0 – 32V and 0 – 6A, respectively. For an output voltage from the power supply unit fixed at 12V (i.e., the typical voltage provided by vehicle batteries), the input current was regulated by the fan's control circuit, which consisted of a set of electrical resistors, providing several step settings

for the fan speeds, i.e., (i) Low, (ii) Medium, (iii) Medium-High, and (iv) High. The corresponding power inputs to the fan, as well as the associated airstream flowrates were measured and summarized in Fig. 16 and Table 2. Three different airflow configurations were tested. First, the downstream heat transfer section, consisting of the evaporator and heater cores, was removed to characterize the original pumping capability of the centrifugal fan (i.e., without any significant sources of pressure drop downstream). Second, the heat transfer section was attached and a dividing lever was flapped to direct the airstream through the evaporator core alone, blocking flow through the heater core. This corresponds to the 'cooling mode' of the ACCS unit wherein the evaporator core attains a temperature below ambient to absorb heat from the airstream. Third, the dividing lever was flapped to direct the airstream through both the evaporator and heater cores. In this configuration, the evaporator core is typically inactive (having an ambient temperature), and the ACCS unit is said to be in the 'heating mode', wherein hot coolant from the engine is pumped through the heater core.

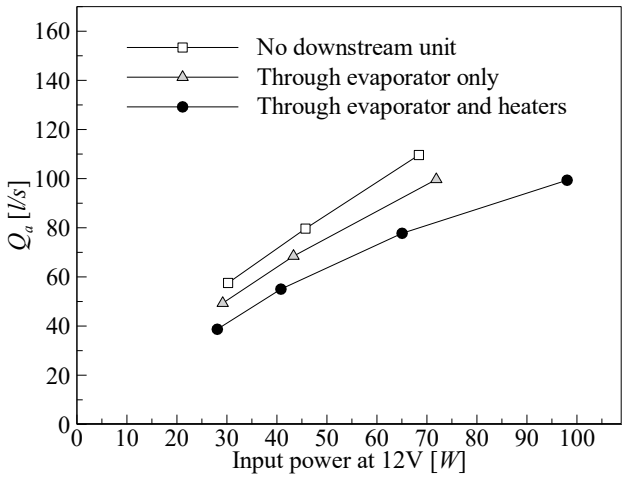


Figure 16. Volume flowrate supplied by the ACCS unit's centrifugal fan at four step input power settings; Low, Medium, Medium-high and High.

The measurement results plotted in Fig. 16 showed that the air volume flowrate was reduced in the presence of the two cores, as expected, due to the increase in flow resistance as the airstream passed through each core. Fig. 16 provided a representative range of airstream flowrates (60 $L/s \leq Q_a \leq 120$ L/s) typically found in ACCS units. These values were used in the current study to fix the range of air-side Reynolds numbers when characterizing the thermo-fluidic performance of a heater core.

To determine the change in flow distribution caused by a given core, time-averaged velocity profiles were measured using a Pitot tube (KIMO, L-type, 3 mm diameter) placed at 0.75 times the tube depth (i.e., $0.75L_t$) downstream of the core as shown in Fig. 17. Two pressure ports of the Pitot tube were connected to a digital micro-manometer (TSI 9565). With a wedge placed immediately upstream of the core, mimicking conditions inside the ACCS unit and blocking off the lower region (i.e., $0 \leq y/H \leq 0.4$), the Pitot tube was traversed from $y = 0$ to $y = H$ along the span-wise centerline of the wind-tunnel, in increments of 0.5 cm

Table 2. Volumetric flowrate based on speed settings, measured in the present study.

Configuration	Speed Setting	Flowrate [*L/s*]
Without downstream unit	Low	57.54
	Medium	79.66
	Medium-High	109.62
Through evaporator only (cooling mode)	Low	49.31
	Medium	68.48
	Medium-High	99.69
Through evaporator and heater (heating mode)	Low	38.71
	Medium	55.04
	Medium-High	77.76
	High	99.36

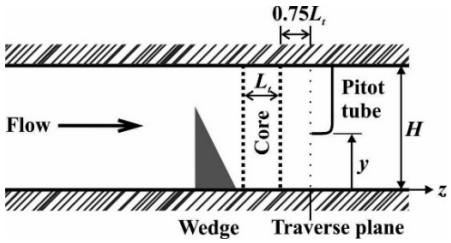


Figure 17. Schematic of wind-tunnel test section showing the downstream traverse plane for a Pitot tube.

2.1.7 Surface flow visualization (Oil-dye technique)

To qualitatively assess the flow behaviour immediately upstream of the core, surface flow visualization was carried out using a light diesel oil/pigment mixture. The mixture was first painted on the back wall (i.e., parallel to the *y*-*z* plane) of the wind tunnel, between the wedge and the louvered fin-tube core, to reveal streak lines in that region. Thereafter, the wind tunnel was turned on, producing a constant airstream flowrate of Q_a = 90 *L/s* (i.e., Re_{lp} = 144). The resulting aerodynamic shear stress on the wall redistributed the oil/dye mixture, causing it to align locally with the direction of the shear stress vector to create a surface flow pattern. Similar to the method reported by Atkins & Boer [35], before application of the mixture, the back wall of the wind tunnel surface was spray-painted with matte black to reduce the reflectivity of the ultraviolet light used to illuminate the dye particles upon imaging.

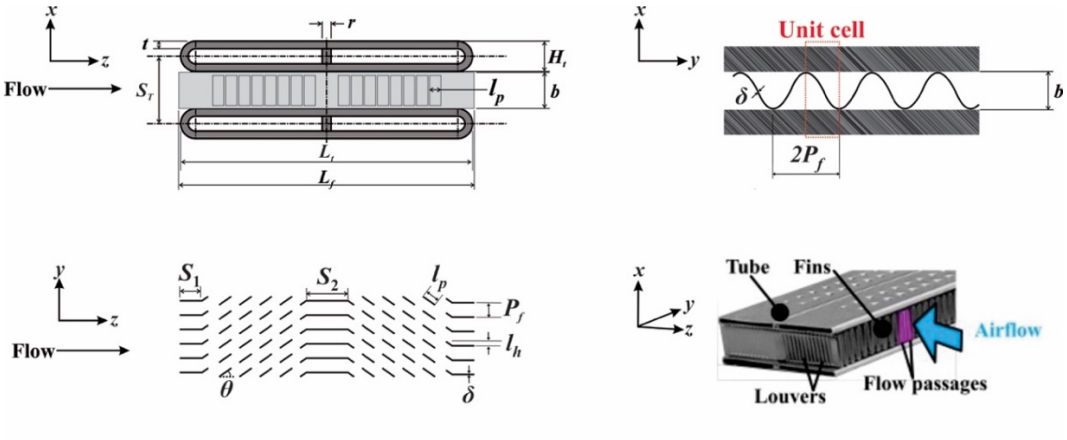
2.1.8 Temperature mapping (IR Thermography)

To obtain temperature distributions of the louvered fin-and-tube heater core, a pre-calibrated infrared camera (FLIR E90) was positioned downstream of the core during operation. The water temperature at the inlet was kept constant at $T_{w,in}$ = 55 °C and the airstream flowrate was maintained at Q_a = 90 *L/s* (i.e., Re_{lp} = 144). Thermal images of the core surface (in the *x*-*y* plane) were obtained at steady-state for both the design condition, as well as the half-ACCS condition, revealing the differences in local cooling performance of the core when operated under uniform and non-uniform incident airstream velocity profiles.

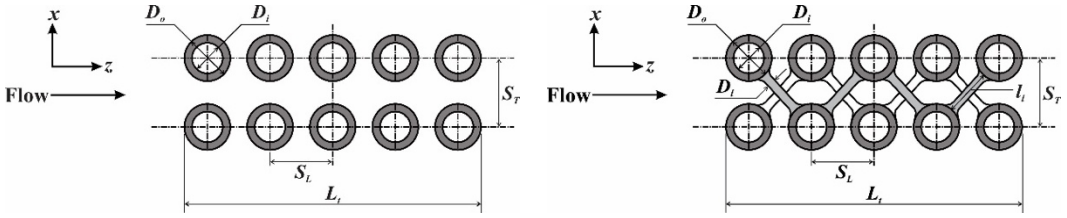
2.2 Heater Core Geometries

Three different heater cores, whose geometries are shown in Fig. 18, were tested in this study. The exact dimensions of each tube, fin, and ligament are detailed in Table 3. Each of the flat tubes (i.e., in Fig. 18(a)), arranged transverse to the cooling airstream, had a cross sectional internal flow area of A_c = 20.8 mm^2 and an external surface area of A_s = 8419 mm^2 whereas each of the circular tube rows (i.e., in Fig. 18(b,c)) consisting of 5 tubes in the flow direction had a total internal cross sectional area of A_c = 18.0 mm^2 and an external surface area of A_s = 7490 mm^2. Both the flat and circular tubes were of equal lengths L = 160 mm along the *y*-axis.

The louvered fins and flat tubes were manufactured conventionally (by Hanon Systems, South Korea) using aluminium sheet metal having a thermal conductivity of k_{al} ~ 205 W/m-K, while the circular tube bank and staggered fin ligaments were manufactured using additive laser sintering (by Renishaw plc, UK) using AlSi10Mg whose thermal conductivity was given as k_{al} ~ 160 W/m-K.



(a)



(b) (c)

Figure 18. Cut-away views showing core dimensions: (a) Louvered fin-and-tube core and unit cell (adopted from Shah & Sekulic [1]), (b) Circular tube bank without fin ligaments, (c) Circular tube bank with staggered fin ligaments (i.e., a lattice porous core).

Table 3. Tubes and fins dimensions.

Component	**Parameter**	**Value (± 0.01 mm)**
Louvered fins	L_f	27.00
	P_f	0.80
	S_1	1.85
	S_2	1.85
	l_p	0.93
	θ	30° ± 0.5°

	δ	0.04
Flat tubes	L_t	27.00
	S_T	7.25
	H_t	1.28
	t	0.40
	r	1.20
Circular ligament	D_l	1.00
	l_l	6.00
Circular tube	S_T	7.25
	S_L	6.00
	D_o	2.98
	D_i	2.14

2.3 Data Processing

2.3.1 Epsilon-NTU method for unmixed cross-flow

The thermal performance of a compact heat exchanger core is commonly reported in terms of the Nusselt number (Nu_x), which first requires determination of the air-side heat transfer coefficient (h_a). Thus, the measured variables ($T_{w,in}$, $T_{w,out}$, $T_{a,in}$, Q_a, and Q_w) were processed using the ϵ-NTU method as follows.

The heat transferred out of the water-stream, $\dot{q}$ is given by:

$$\dot{q} = \dot{m}_w c_{p,w}\left(T_{w,in} - T_{w,out}\right) \tag{1}$$

where $\dot{m}_w$ is the mass flowrate of the water, $c_{p,w}$ is the specific heat capacity, and $T_{w,in}$ and $T_{w,out}$ respectively represent the water temperatures at the inlet and outlet of the core's header tubes.

Since there is a finite difference between the water and airstream temperatures, which decreases as the streams pass through the heat exchanger, the maximum amount of heat which can be transferred between the streams is limited and is only achievable in principle with a counter-flow heat exchanger of infinite length. In this case, the maximum theoretically achievable heat transfer rate, from the heated water to the airstream, would be:

$$\dot{q}_{max} = C_{min}\left(T_{w,in} - T_{a,in}\right) \tag{2}$$

where $C_{min} = \min(C_a, C_w)$ and $T_{a,in}$ is the temperature of the air measured upstream of the core. C_a and C_w are the heat capacity rates of the air and water-streams, respectively, and are defined as:

$$C_a = \dot{m}_a c_{p,a} = \rho_a Q_a c_{p,a} \tag{3}$$

$$C_w = \dot{m}_w c_{p,w} = \rho_w Q_w c_{p,w} \tag{4}$$

where $\dot{m}$, c_p, ρ, and Q respectively represent the mass flow rate, specific heat capacity, density, and volumetric flow rate of the associated fluid; the subscripts a and w refer to the air- and water-streams respectively. Note that $C_{min} = \min(C_a, C_w)$ is always used in Eq. 2 instead of $C_{max} = \max(C_a, C_w)$, because energy conservation requires that the fluid with the lower heat capacity rate experiences the larger temperature change.

The definition of a heat exchanger's effectiveness (ϵ), i.e., the ratio between the actual heat transfer rate and the theoretical maximum and is defined as:

$$\epsilon = \frac{\dot{q}}{\dot{q}_{max}} \tag{5}$$

from which the number of transfer units (NTU) for single pass cross flow conditions with both fluids unmixed can be solved iteratively using the following relation [2]:

$$\epsilon = 1 - exp\left(\frac{NTU^{0.22}}{C_r}\{exp[-C_r(NTU)^{0.78}] - 1\}\right) \tag{6}$$

where

$$C_r = \frac{C_{min}}{C_{max}} = \frac{\min(\mathrm{C_a}, \mathrm{C_w})}{\max(\mathrm{C_a}, \mathrm{C_w})} \tag{7}$$

From the definition of *NTU*, one may calculate the overall heat transfer coefficient *U* based on the total air-side heat transfer surface area A_a, as:

$$U = \frac{C_{min} NTU}{A_a} \tag{8}$$

In this case, A_a was calculated using a unit cell approach, as follows. From Fig. 18(a), the primary tube surface area per unit cell, is:

$$A_{p,cell} = 2L_t\left(P_f - \delta\right) + 2P_f H_t \tag{9}$$

and the fin surface area per unit cell is:

$$A_{f,cell} = 2L_f\left(\sqrt{b^2 + P_f^2} - \delta\right) \tag{10}$$

where the term in brackets represents the diagonal height of the fin along its centerline. The number of unit cells, n_{cells}, is given by:

$$n_{cells} = N_p\left(\frac{W}{P_f}\right) \tag{11}$$

where $N_p = 31$ is the total number of fin passes, i.e., sandwiched between flat tubes, and the term in brackets represents the number of airflow passages (shown in Fig. 5) between the fins. Thus,

$$A_a = n_{cells}(A_{p,cell} + A_{f,cell}) \tag{12}$$

2.3.2 Air-side heat transfer coefficient

To calculate h_a, a one-dimensional steady-state surface energy balance, assuming negligible fouling resistance and constant thermo-physical properties was used as follows:

$$h_a = \frac{1}{\eta_0}\left\{\frac{1}{U} - A_a R_{cond} - \frac{A_a}{A_w h_w}\right\}^{-1} \tag{13}$$

where η_o is the fin surface efficiency, R_{cond} is the conduction resistance through the tube wall, h_w is the water-side heat transfer coefficient, and A_w is the total inner surface area of the tubes.

2.3.3 Fin efficiencies for louvered and cylindrical fin geometries

For un-finned surfaces, $\eta_o = 1$ whereas for a finned surface in general η_o is given by

$$\eta_0 = 1 - \frac{A_f}{A_a}(1 - \eta_f) \tag{14}$$

where A_f represents the total surface area of the fins and the fin efficiency η_f is:

$$\eta_f = \frac{\tanh(ml)}{ml} \tag{15}$$

For a louvered fin geometry, on the airside [1],

$$m = \sqrt{\frac{2h_a}{k_{al}\delta}\left(1 + \frac{\delta}{L_f}\right)} \tag{16a}$$

and

$$l = \frac{\left(\sqrt{b^2 + P_f^2} - \delta\right)}{2} \tag{16b}$$

where k_{al} is the thermal conductivity of the fin material, δ is the fin thickness, L_f is the fin length in the flow direction, b is the fin height, and P_f is the fin pitch.

For a cylindrical fin geometry, on the airside we have [2]

$$m = \sqrt{\frac{4h_a}{k_{al}D_l}} \tag{17a}$$

and

$$l = l_l + \frac{D_l}{4} \tag{17b}$$

where D_l is the fin ligament diameter and l_l is the fin ligament length.

2.3.4 Tube conduction resistances

Tube-wall conduction resistances are dependent on the tube geometry. For the flat tubes found in the louvered fin core, total wall conduction resistance was approximated as that through a plane wall. Thus

$$R_{cond} = N_t \frac{t}{k_{al}A_{wall}} \tag{18a}$$

where N_t is the total number of tubes, t is the tube thickness, k_{al} is the tube's thermal conductivity, and $A_{wall} = L \times L_t$ is the area of the flat surface of the tube. For circular tubes found in the lattice porous core, conduction resistance is given by:

$$R_{cond} = N_t \frac{\ln\left(\frac{D_o}{D_i}\right)}{2\pi k_{al} L} \tag{18b}$$

where D_o, D_i, and L respectively represent the outer diameter, inner diameter, and the length of the tube.

2.3.5 Water-side heat transfer coefficient

For the waterside Nusselt number Nu_w of the high aspect ratio flat tubes, the following analytical correlation, adopted from Shah & Sekulic [1], which assumes laminar fully developed conditions, constant axial wall heat flux, and constant peripheral wall temperatures prevailing throughout the tube length:

$$Nu_w = 8.235(1 - 2.0421\alpha^* + 3.0853\alpha^{*^2} - 2.4765\alpha^{*^3} + 1.0578\alpha^{*^4} - 0.1861\alpha^{*^5}) \tag{19a}$$

where

$$\alpha^* = \frac{H_t - 2t}{\frac{1}{2}(L_t - 2t - r)}$$

H_t is the tube height, L_t is the tube width, and r is the center rib thickness.

For circular tubes, the general solution to the energy equation, assuming laminar fully developed flow in the tubes and uniform surface heat flux, was used as follows [2, 8]:

$$Nu_w = 4.36 \tag{19b}$$

Once the water-side Nusselt numbers were calculated for the different tube geometries, the heat transfer coefficient h_w could be extracted using the definition:

$$h_w = \frac{k_w}{D_{h,t}} Nu_w \tag{20}$$

where k_w is the thermal conductivity of water and $D_{h,t}$ is the internal hydraulic diameter of the tube.

2.3.6 Colburn j-factor and selection of a characteristic length

Equations 13 to 17 were solved iteratively for both of the finned surfaces, starting with $\eta_o = 1$ and refining the heat transfer coefficient h_a until convergence of η_o was achieved to within 10^{-6}. Thereafter, the air-side Nusselt number Nu_x based on a characteristic length x was computed as:

$$Nu_x = \frac{h_a x}{k_a} \tag{21}$$

where, conventionally, $x = l_p$, for a louvered fin core and $x = D_o$ for a cylinder bank.

Once the airside Nusselt number was obtained, the corresponding Colburn j-factor was computed using the definition:

$$j_x = \frac{Nu_x}{Re_x Pr^{1/3}} \tag{22}$$

for consistent comparison between the current experimental data and the correlations developed previously in the literature.

When comparing the performance of the louvered fin-and-tube core against results in the literature, the conventional characteristic length scale (i.e., $x = l_p$) was used for consistency with the literature. In this case, the Reynolds number, Re_{lp}, was calculated using the maximum velocity, u_0, through the core's minimum flow-facing cross-sectional area, i.e., the bulk air flowrate Q_a divided by the total free-flow area through the core, A_0, which is found by using the unit cell (Fig. 18(a)) approach as follows:

$$A_0 = n_{cells} A_{0,cell} = n_{cells} \left[b P_f - \delta \left(\sqrt{b^2 + P_f^2} - \delta \right) \right] \tag{23}$$

where n_{cells} is given by Eq. 11. Therefore,

$$Re_{lp} = \frac{\rho \left(\frac{Q_a}{A_0} \right) l_p}{\mu_a} \tag{24}$$

When making comparisons between the different heater cores used in this study, the hydraulic diameter of the wind tunnel, D_h, was used as a characteristic length scale (i.e., $x = D_h$) for consistency between the different core geometries. In this case, the Reynolds number, Re_{Dh}, was calculated using the average bulk velocity of the airstream upstream of the core, i.e., the bulk flowrate Q_a divided by the tunnel cross-sectional area (WH). Thus:

$$Re_{Dh} = \frac{\rho \left(\frac{Q_a}{WH} \right) D_h}{\mu_a} \tag{25}$$

where $D_h = \frac{4WH}{2(W+H)}$.

2.4 Uncertainty Analysis

2.4.1 Absolute uncertainties of measurement instruments

Experimental parameters in this study were measured using physical instruments, each having a distinct uncertainty associated with their measurement. These 'absolute' uncertainties, listed in Table 4, propagated through the mathematical operations of the data processing method to produce cumulative uncertainties in the final derived variables.

Table 4: Absolute uncertainties of measurement instruments used in this study.

Parameter	**Measurement instrument**	**Absolute uncertainty [unit]**
Fin thickness, δ	Micrometer screw gauge	$\pm 1\times 10^{-6}$ [m]
Tube thickness, t	Vernier caliper	$\pm 2\times 10^{-5}$ [m]
Tube height, H_t		
Fin depth, L_f		
Louver pitch, l_p		
Fin pitch, P_f		
Fin height, b		
Tube radius, r		
Core width, W		
Tube depth, L_t		
Atmospheric pressure, P_o	Digital barometer	$\pm$ 0.1 [kPa]

Air flowrate, Q_a	Turbine flow-meter	± 0.1 [L/s]
Water flowrate, Q_w	Turbine flow meter	± 2.25× 10^{-3} [L/s]
Air inlet temperature, $T_{a,i}$	T-type thermocouple	± 0.01 [ºC]
Water inlet temperature $T_{w,i}$		
Water outlet temperature, $T_{w,o}$		

2.4.2 Propagation of absolute uncertainties through data processing

If $y = f(x_1, x_2, \ldots, x_n)$ then the uncertainty propagated by x_i in the derived quantity y is given by [36]:

$$\Delta y = \sqrt{\left(\frac{\partial y}{\partial x_1}\Delta x_1\right)^2 + \left(\frac{\partial y}{\partial x_2}\Delta x_2\right)^2 + \cdots + \left(\frac{\partial y}{\partial x_n}\Delta x_n\right)^2} \tag{26}$$

where Δx_i is the absolute uncertainty in the measurement of x_i. Equation 26 was used to estimate the overall experimental uncertainties associated with steady-state temperature and flowrate measurements. Thus, using Eqns. 21-24 and the absolute uncertainties (Table 4), the maximum relative uncertainty propagated in the calculations of Nusselt number, Reynolds number, and Colburn j-factor, respectively, were 13.0%, 2.5%, and 12.9% for the range of air and water flowrates considered in this study. These uncertainties were consistent with the range of uncertainties commonly encountered in compact heat exchanger literature that used the same steady-state measurement technique [34].

3 DISCUSSION OF RESULTS

This chapter first verifies that the experimental method and apparatus, described in the preceding chapter, produced reliable data. This is done by comparing the design performance data of the louvered fin-and-tube heater core with correlations established in the literature. Thereafter, the thermal performance deterioration experienced by the louvered fin-and-tube heater core, inside the ACCS unit, is quantified. The physical mechanism responsible for this deterioration is explained by considering experiments carried out in the modified wind tunnels, which incrementally simulated conditions inside the ACCS. The lattice porous core is shown to overcome the thermal performance deterioration at off-design conditions, and the reasons behind this are explained by comparing the thermal and hydraulic dispersion characteristics of the two cores. Finally, the effect of the lattice porous core's circular fin ligaments on thermal and hydraulic dispersion of a non-uniform airstream, are shown to be key in improving its thermal performance under off-design conditions.

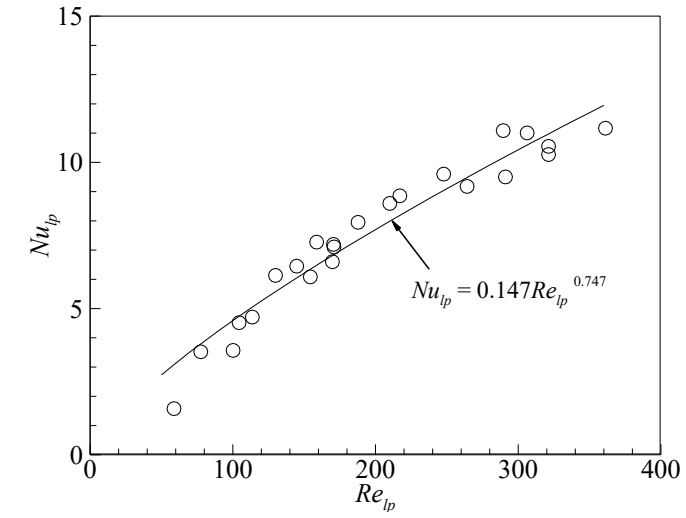
3.1 Thermo-Fluidic Performance of a Louvered Fin-and-Tube Heater Core

3.1.1 At design conditions (verification of experiments)

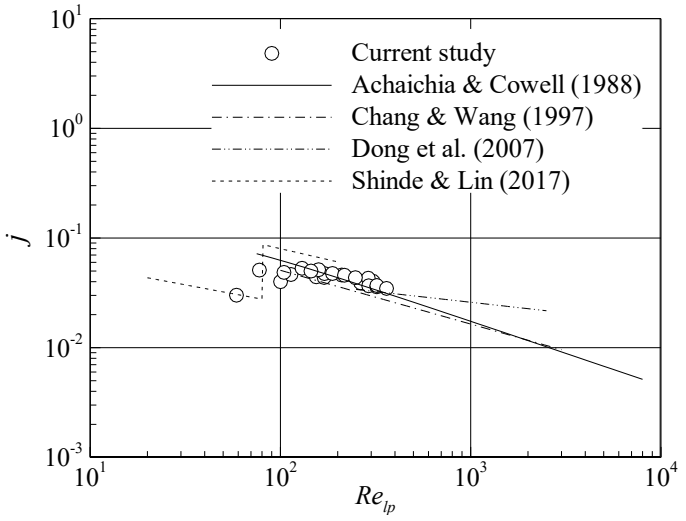
A reference case, to determine the credibility of the test setup, was established by placing a louvered fin-and-tube heater core in a uniform, unidirectional airstream without any upstream or downstream obstructions (Fig. 6). This setup conformed to the experimental conditions adopted by previous researchers [19, 24, 25]. Under these conditions, steady-state temperature measurements were taken for the range of air volume flowrates, $36.6\ L/s \leq Q_a \leq 225\ L/s$, which encompasses the range of flowrates typically encountered in an ACCS unit (i.e., $60 \leq Q_a \leq 120\ L/s$). The corresponding Reynolds number range, based on louver pitch, was $58.8 \leq Re_{lp} \leq 361$, for which the steady-state Nusselt number (Nu_{lp}) variation is shown in Fig. 19(a). Converting Nu_{lp} in the power law correlation of Fig. 19(a) to Colburn j-factor using Eq. 22 yields $m = -0.253$ for the exponent of Re_{lp}, which is reasonably close to other correlations reported in the literature (Table 1). As shown in Fig. 19(a), the correlation $Nu_{lp} \propto Re^{0.747}$, where the exponent is between 0.5 and 0.8, is typically indicative of heat transfer due to transitional flow (i.e., transition from laminar to turbulent flow, in this case) [2]. This is in line with the observations of both DeJong & Jacobi [24] and Tafti et al. [21], that laminar flow with unsteadiness exists throughout the louver array at $Re_{lp} > 100$, which rules out the possibilities of heat transfer due to either purely laminar or purely turbulent flow. Discrepancies in the exact magnitude of the correlation exponent are due to the different louver geometries used in previous studies, which account for varying degrees of the flow unsteadiness and flow efficiency at a given Reynolds number [18, 20, 26]. Nonetheless, the indication of laminar to turbulent transitional flow is consistent, both in this work and among previous researchers (e.g., Table 1).

Figure 19(b) shows the variation of Colburn j-factor (j) with Re_{lp}, obtained experimentally for the louvered fin-and-tube heater core in this study, versus the correlations developed in previous studies

[19, 22, 24, 25]. In the range of Reynolds numbers $130 \leq Re_{lp} \leq 361$, Achaichia & Cowell's [19] prediction was in line with the experimental data, having a maximum deviation of 13.2% while the rest of the points were within the reported correlation precision of 10%. The other correlation valid in the abovementioned Reynolds number range, due to Chang & Wang [22], had significant deviation from the experimental data (up to 26%). This discrepancy likely stemmed from the fact that the data bank used by Chang & Wang consisted of a variety of cores with different types of louvered fins, including corrugated fins with triangular and rectangular channels, corrugated fins with splitter plates, as well as plain plate fins. Nevertheless, important trends in the experimental data were consistent, and it was therefore assumed that reliable comparisons in thermal performance, between design and off-design conditions could be made against these results.

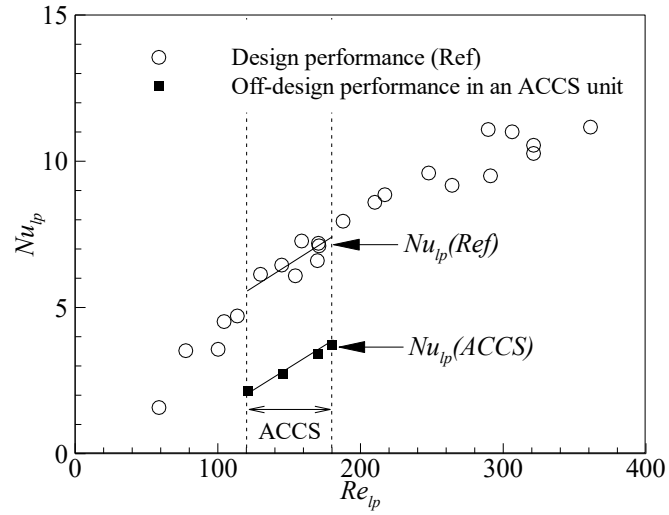


(a)

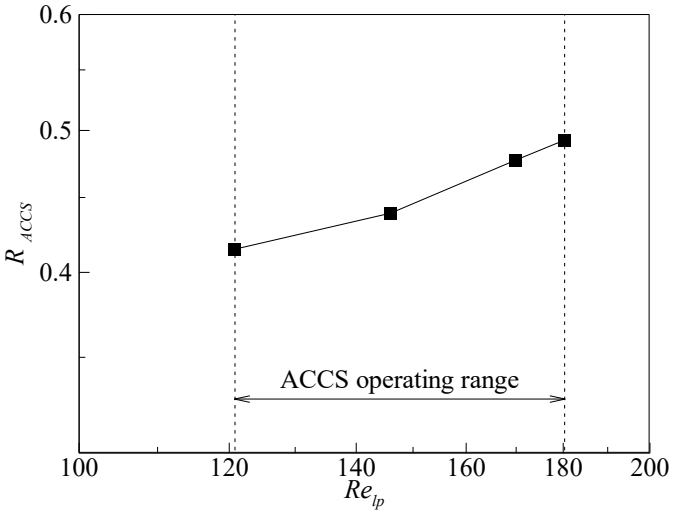


(b)

Figure 19. Design performance of a louvered fin-and-tube heater core: (a) Nusselt number (Nu_{lp}) variation with Reynolds number (Re_{lp}), (b) Colburn j-factor (j) variation with Reynolds number (Re_{lp}), relative to previous correlations.



(a)



(b)

Figure 20. Comparison of thermal performance of a louvered fin-and-tube heater core operating under design and off-design conditions (i.e., inside the ACCS unit): (a) Variation of Nusselt numbers measured at design conditions ($Nu_{lp}(Ref)$) and off-design conditions (Nu_{lp} $(ACCS)$) with louver pitch-based Reynolds number (Re_{lp}), (b) Variation of $Nu_{lp}(ACCS)$ with Re_{lp}, normalized by $Nu_{lp}(Ref)$.

3.1.2 At off-design conditions (inside an ACCS)

By placing the louvered fin-and-tube core inside the ACCS unit (Fig. 14) and taking steady-state temperature and flowrate measurements, the thermal performance of the core was characterized under a combination of off-design conditions, i.e., with non-uniform, obstructed flow upstream of the core and ducting (which imposes flow redirection and area change) downstream of the core. Measurements were obtained for the range of air volume flowrates produced by the unit's centrifugal fan at each of its four step settings (i.e., Low, Medium, Medium-High, and High as specified in

Table 2) when the unit was configured in its heating mode. The corresponding Reynolds number range was $121 \leq Re_{lp} \leq 180$, for which the variation of Nusselt number, i.e., $Nu_{lp}(ACCS)$, is compared with the design setup, i.e., $Nu_{lp}(Ref)$ in Fig. 20(a). The combination of off-design conditions clearly resulted in significant reduction in thermal performance. In ascertaining the effect of Reynolds number on this reduction, a performance ratio, R_{ACCS}, measuring the deviation of the Nusselt number from the design setup (acting as a reference value) was defined as:

$$R_{ACCS} = \frac{Nu_{lp}(ACCS)}{Nu_{lp}(Ref)} \tag{27}$$

The variation of R_{ACCS} with Re_{lp} is plotted in Fig. 20(b) from which it can be seen that at lower Reynolds numbers, corresponding to low and medium fan speeds of the ACCS, the difference between design and off design performance was ~60% while at higher fan speeds the performance deviation was ~50%. The effect of thermal performance degradation was more pronounced at lower Reynolds numbers, and this could be due to a reduction in the total mass-flowrate of 'clean' (or uniform) air incident on the core. Such a severe drop in overall thermal performance, i.e., 50% ~ 60%, could not be attributed directly to any individual off-design condition reported in previous literature. Therefore, simply superimposing the effects of plausible off-design configurations previously reported may prove to be misleading. In fact, some configurations (such as non-uniform external coolant stream) were reportedly detrimental to heat transfer while other configurations (such as external coolant stream's inclination) were favourable to heat transfer [17, 23]. As a result, it was difficult to pin-point the exact cause(s) of the performance reduction with only the performance data in Fig. 20.

There is merit, however, in identifying the causes of thermal performance reduction in the ACCS. Future design iterations may better account for the deviation and allow for more efficient operation of the unit. Therefore, performance was further investigated by modifying the wind tunnel, used for the reference case, to incrementally mimic the setup within the ACCS unit as shown schematically in Figs. 15(a) and (b). In this way, the individual contributions of key geometrical features of the ACCS configuration, to the performance deviation, could be determined.

3.1.3 At simulated ACCS unit conditions

Airflow upstream of the core

In modifying the wind tunnel setup to mimic that of the ACCS unit, a wedge obstruction was placed upstream of the core (Fig. 15(a)). This setup was seen to mimic only the conditions upstream of a heater core placed inside the ACCS unit, i.e., without any downstream ducting, as shown schematically in Fig. 21. This setup is referred to as "half-ACCS unit" conditions. Nusselt numbers obtained under half-ACCS unit conditions ($Nu_{lp}(h)$), for the ACCS unit's applicable range of Reynolds numbers $121 \leq Re_{lp} \leq 180$, were normalized by $Nu_{lp}(Ref)$. This yielded the performance

ratio $R_h = Nu_{lp}(h)/Nu_{lp}(Ref)$ which is plotted along with R_{ACCS} and the reference/design performance in Fig. 22. A thermal performance reduction of up to 32% relative to the reference case was noted.

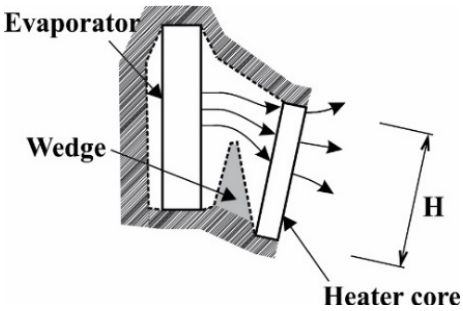


Figure 21. Schematic representation of air flow inside an ACCS unit without ducting downstream of the core (i.e., half-ACCS unit).

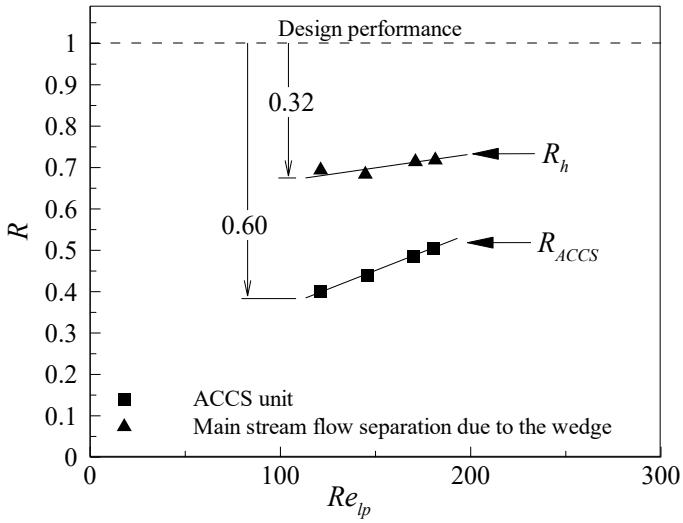
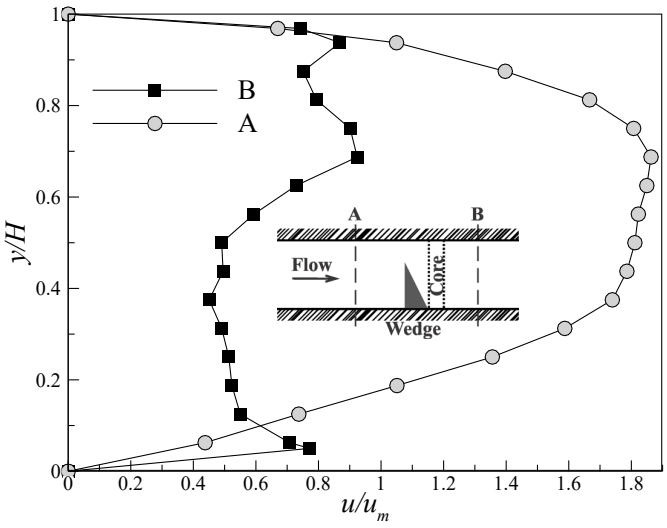
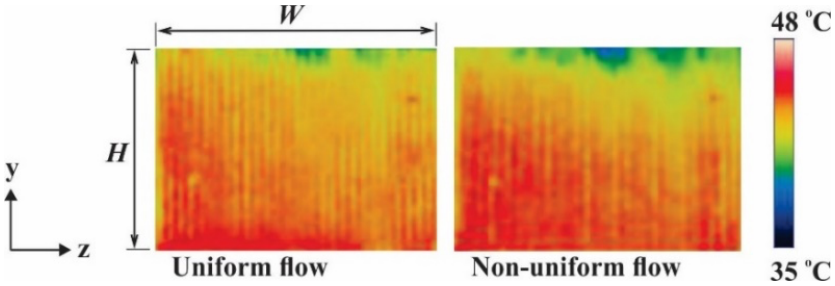


Figure 22. Influence of the wedge obstruction alone on the thermal performance of a louvered fin-and-tube heater core.

Based on the results of T'Joen et al. [14], Datta et al. [15], and Blecich [16], it was suspected that the external coolant stream's non-uniformity upstream of the core, caused by the wedge obstruction, resulted in the thermal performance deterioration. The airstream non-uniformity was quantified by measuring the airstream velocity profiles upstream and downstream of the wedge-core combination, as shown in Fig. 23(a), and its effect on the reduction of heat transfer performance was characterized as follows. The upstream flow (denoted as "A" in Fig. 23(a)) was skewed slightly due to the presence of the wedge. The flow was channelled between the apex of the wedge and the channel upper wall. The downstream flow (denoted as "B" in Fig. 23(a)), was distributed with a relatively high concentration of airflow towards the upper region ($0.7 \leq y/H \leq 1.0$), indicating that the core experienced a large flux of cool airstream in the upper region while majority of the core experienced a much lower flux. The result was that only the upper fraction of the core's surface was used effectively for transferring heat to the airstream.



(a)



(b)

Figure 23. Effect of an upstream wedge on the thermal performance of a louvered fin-and-tube heater core: (a) Velocity profiles for Re_{lp} = 180, measured at A = 0.3H upstream from the wedge and at B = 0.2H downstream from the heater core, (b) Infrared thermographs of the heater core showing the effect of non-uniform incident coolant flow on the temperature distribution of the core.

To supplement the foregoing analysis, infrared temperature maps of the core, operating both under reference conditions and under half-ACCS unit conditions, were obtained. In both cases, the inlet water temperature and air volume flowrate were kept constant at $T_{w,in}$ = 45 °C and Q_a = 90 L/s (or Re_{lp} = 144), respectively. The resulting thermographs are shown in Fig. 23(b), where the temperature distributions on the core surface, for the reference case and the half-ACCS unit case, can be compared. Hot water enters at the lower end of the core (y/H = 0) and flows upward (in the positive y-direction) as the airstream, flowing perpendicular to the image (in the x-direction), cools the core. When the airflow is uniform, a small region near y/H = 0 is at the inlet water temperature $T_{w,in}$, after which the water-stream is gradually cooled as it traverses the span of the core (H). In contrast, with a wedge upstream, gradual cooling of the water-stream is only evident towards the upper core region (y/H > 0.5) due to higher-momentum flow in the region 0.7 ≤ y/H ≤ 1.

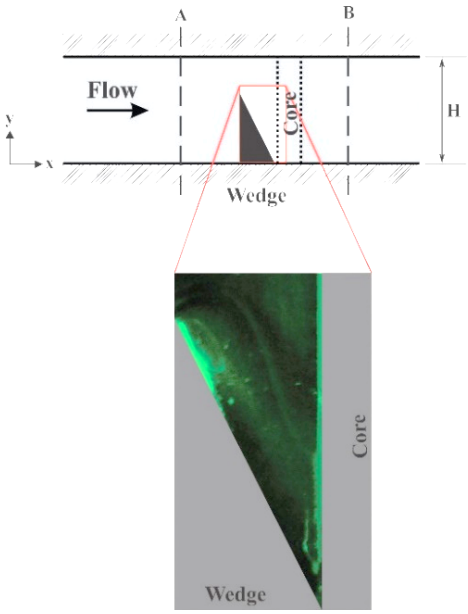


Figure 24. Flow visualization image showing separated flow marked by a bright region of accumulated dye particles.

The total thermal performance deterioration (~30%) could not be due to the non-uniform airstream alone. Blecich [16] reported a 30% thermal performance deterioration only for extremely non-uniform airflows, where part of the core (particularly, $0 \leq y/H \leq 0.33$) was completely covered, blocking the airstream from entering the core in that region. For all other cases, where the entirety of the core was exposed to the airstream, the thermal performance deterioration did not exceed 18%.

End-wall flow visualization, shown in Fig. 24, was carried out to discern any possible flow mechanism(s) responsible for further reduction in thermal performance. Separation (marked by a bright region of accumulated dye particles) occurred at the wedge apex, in proximity with the core. This separation was expected, due to the sharp turning angle for the flow downstream of the wedge. As a result of separation, a shear layer encloses air in the lower region of the core (i.e., approximately $0 \leq y/H \leq 0.4$). The shear layer blocks low-temperature mainstream flow from entering the core in the lower region, similar to the extreme case of Blecich [16], causing the marked thermal performance deterioration noted in Fig. 23. Therefore, non-uniform flow which induces duct-directed flow within parts of the louvered fin-and-tube core (see Fig. 10), as well as separation which effectively blocks off a region of the core from the fresh coolant stream, are both responsible for approximately half of the total thermal performance reduction in ACCS units.

Airflow downstream of the core

Vertical ducting downstream of the heater core was suspected at further contributing towards the total thermal performance reduction. To test this, both upstream and downstream conditions were mimicked in the wind tunnel as shown in Fig. 15(b). This situation corresponded to the “full-ACCS unit” conditions.

Since velocity and infrared measurements downstream of the core, with a narrow duct in place, were impractical, only steady-state temperature and flowrate measurements were carried out for the full-ACCS unit case. The average Nusselt numbers obtained under full-ACCS unit conditions, $Nu_{lp}(e)$, were normalized by the reference case Nusselt numbers, leading to the performance ratio $R_e = Nu_{lp}(e)/Nu_{lp}(Ref)$ which is plotted along with R_h and R_{ACCS} in Fig. 25

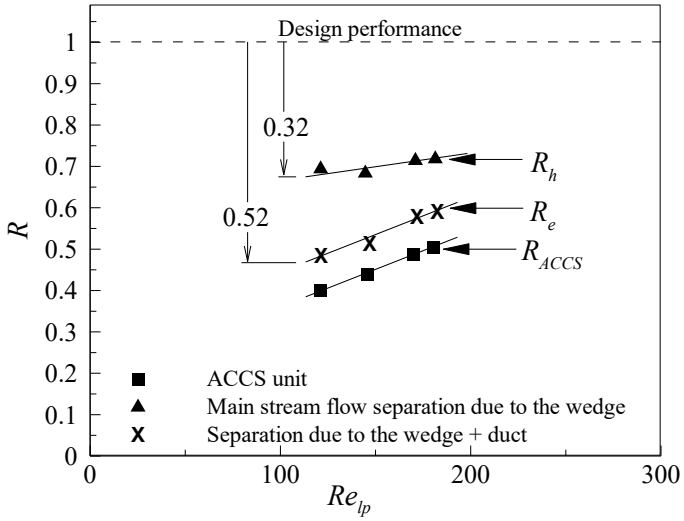


Figure 25. Combined influence of the wedge obstruction and downstream ducting on the thermal performance of a louvered fin-and-tube heater core.

Due to upward turning of the airstream downstream of the core, the thermal performance of the core under full-ACCS unit conditions decreased by a further 20%, approaching that of the actual off-design conditions to within 10%. This was likely due to recirculation of warm air in the lower region downstream of the core, as shown schematically in Fig. 26, which reduced the overall temperature gradient and heat transfer rate between the core and the airstream in that region. The recirculating flow eventually reached its saturation point for extracting heat from the core, and this manifested as the observed thermal performance reduction at steady-state.

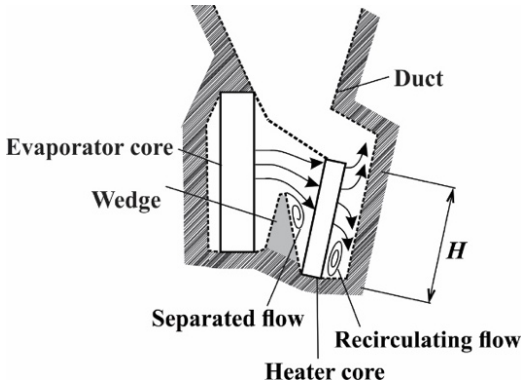


Figure 26. Schematic representation of separated and recirculating flow regions inside an ACCS unit.

3.2 Hydraulic Dispersion

3.2.1 In a louvered fin-and-tube core

When a non-uniform airstream is incident on the louvered fin-and-tube core, different parts of the core receive local cooling airstreams having dissimilar mass fluxes. As a result, different portions of the core experience different levels of heat transfer – lower heat transfer in regions of low local mass flux, and higher heat transfer in regions of high local mass flux. In this case, the heat transfer surface area of the core is not fully utilized. To circumvent this issue, the non-uniform airstream must be redistributed or spread out, i.e., "dispersed", across the core. Ideally, this would enable all parts of the core to experience equal local mass fluxes of the cooling airstream, in turn, enabling all parts of the core to equally participate in heat transfer to ensure full utilization of the available core surface area. In this context, "hydraulic dispersion" refers to redistribution of fluid momentum during the passage of an external airstream through the heater core, as illustrated in Fig 11.

To determine the hydraulic dispersion characteristics of a particular core, the velocity distributions of the airstream upon entering and exiting the core were measured by traversing a Pitot tube laterally (from $y = 0$ to $y = H$) along the mid-span of the wind-tunnel. Having only a wedge upstream of an empty test section (i.e., without any core inserted), Fig. 27 shows that the wedge blockage reduced the local cross-sectional flow area in the upper region ($0.6 \leq y/H \leq 1.0$), resulting in a local acceleration in that region. The dip in velocity at $y/H = 0.78$ followed by an increase and then gradual decrease in velocity as y/H decreased was likely due to the shear layer following separation at the wedge apex (Fig. 24). When the core was placed inside the test section, the high-momentum fluid in the region $0.6 < y/H < 1.0$ impinged the louvered fin-and-tube core, and a portion of the airstream travelled through the fin passages (each of width P_f) to exit the core on the opposite side. Aerodynamic resistance in the longitudinal (z) direction caused the remaining portion to turn downward (in the negative y-direction), upstream of the core. Some of this fluid was pushed through the fin passages (at a lower longitudinal velocity) on its way towards the bottom wall of the wind-tunnel. The rest exited as a jet-like structure through a relatively wide opening found between the core's bottom-most fin and header tube, as seen near $y/H = 0.03$. In this way, the louvered fin-and-tube heater core exhibited hydraulic dispersion, albeit in a very limited amount and occurring only outside of the core. The airflow could not have traversed the lateral direction while passing through the louvered fin-and-tube core, because the deflection and turnaround louvers of the fins (i.e., S_1 and S_2 respectively in Fig. 18(a)) are known to direct incident airstreams along their lengths [20]. Thus, the exit velocity profile remained non-uniform and had a similar shape to the inlet velocity profile.

The louvered fin-and-tube core's resistance to flow in the lateral (y) direction caused fluid that passed through the lower region of the core ($0.1 \leq y/H \leq 0.6$) to have relatively low velocity in the z-direction. As a result, the airflow structure inside the fins likely changed from louver-directed at

the top of the core, to duct-directed (which decreased thermal performance) at the bottom of the core, as illustrated in Fig. 10.

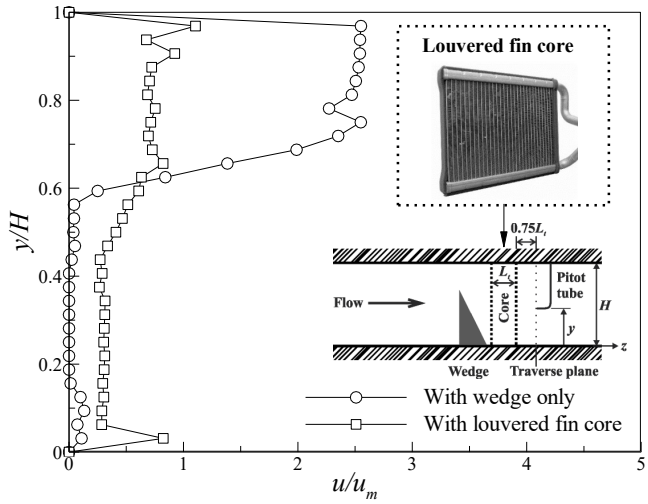
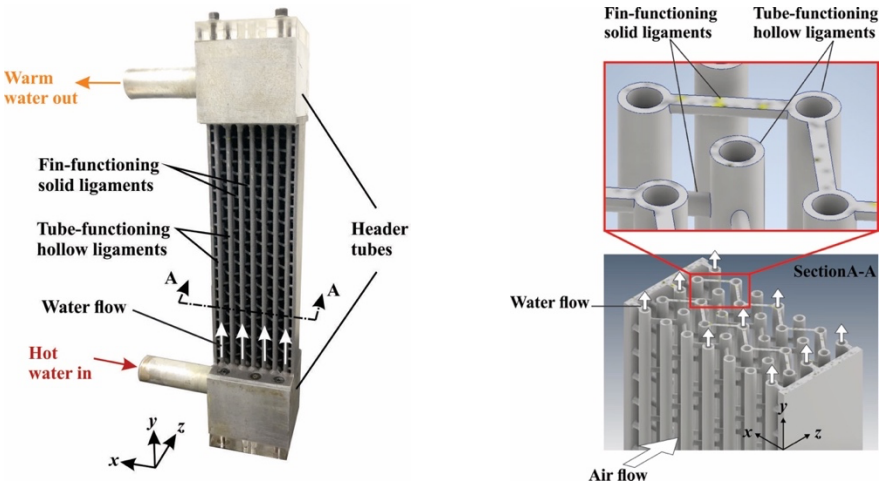


Figure 27. Velocity profiles measured at 0.75L_t downstream of a louvered fin-and-tube core with a wedge placed immediately upstream as indicated in the inset.

3.2.2 In a lattice porous core (influence of aerodynamic anisotropy)

To improve hydraulic dispersion (and therefore heat transfer to the airstream), it was important that the airstream was able to travel laterally across the fins, while passing through the core, such that the non-uniform flow upstream would not persist downstream of the core. Thus, the core required suitable aerodynamic anisotropy, which was achieved by using a "lattice porous" core consisting of circular pin-fin ligaments running horizontally in the transverse (x) direction, each attached to laterally (y-direction) running cylindrical tubes, as shown in Fig. 28.



(a) (b)

Figure 28. Lattice porous heater core: (a) Assembled core with header tubes, (b) Cut-away view in the x-z plane (A-A).

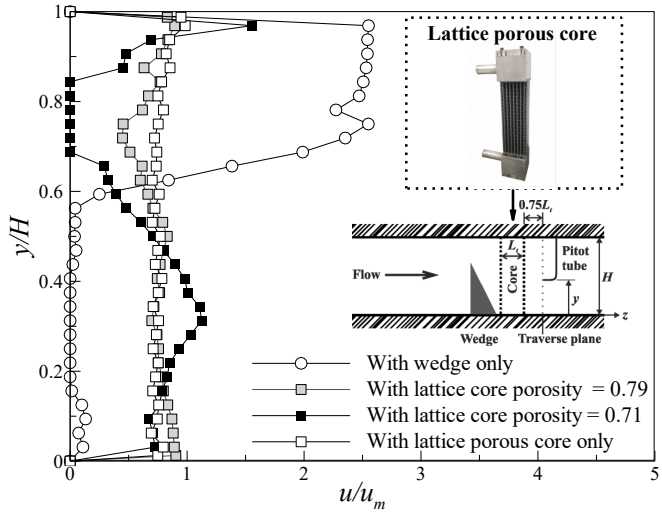


Figure 29. Velocity profiles 0.75L_t downstream of a lattice porous heater core with a wedge placed immediately upstream as indicated in the inset.

The lattice porous core, manufactured by additive laser sintering, was placed under half-ACCS unit conditions i.e., inside the test section of a wind-tunnel with only a wedge obstruction upstream (as shown in Fig. 15(a)). A Pitot tube was traversed laterally, downstream of the core (Fig.17), and Fig. 29 shows the effect of the lattice porous core's inherent aerodynamic anisotropy on hydraulic dispersion. Particularly, a lattice porous core with porosity of 0.71 "reversed" the non-uniform incident velocity profile caused by the wedge, because the aerodynamic resistance of the fin ligaments, which form a staggered tube bank when viewed through the *y*-*z* plane (as shown in Fig. 11), was significantly larger in the longitudinal (*z*) direction compared to the lateral (*y*) direction. As a result, the core forced flow downward (in the negative *y*-direction), resulting in the re-distributed (i.e., "reversed") exit velocity profile. When the porosity of the lattice porous core was increased to 0.79, by reducing the diameter of the fin-functioning ligaments, aerodynamic resistance in the longitudinal (*z*) direction was reduced, resulting in a relatively more uniform exit velocity profile.

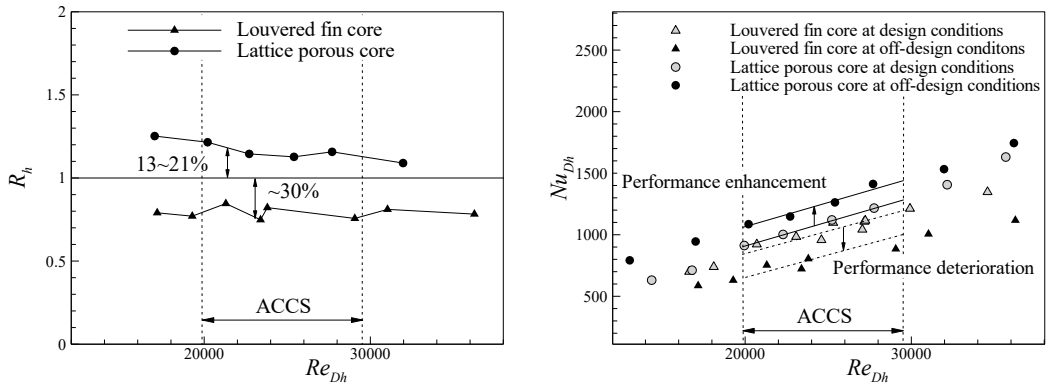
3.3 Thermo-Fluidic Performance of a Lattice Porous Core

3.3.1 At design and off-design conditions

Under half-ACCS unit conditions, up to ~30% decrease in thermal performance was noted for the louvered fin-and-tube core, as shown in Fig. 30(a), where R_h represents a normalized performance ratio defined as:

$$R_h = \frac{Nu_{Dh}\ at\ half\ ACCS\ unit\ conditions}{Nu_{Dh}\ at\ design\ conditions} \tag{22}$$

Nu_{Dh} is the Nusselt number based on the hydraulic diameter of the wind tunnel, D_h. With the lattice porous heater core (having a porosity of 0.79) placed under the same conditions, a 13~21% thermal performance enhancement was noted instead.



(a) (b)

Figure 30. Overall thermal performance comparison between a louvered fin-and-tube core and a lattice porous core operating at off-design conditions, simulated by the half-ACCS wind tunnel configuration: (a) Normalized performance variation with Re_{Dh}, (b) Nusselt number variation with Re_{Dh}.

At design conditions, the thermal performance of both cores was similar, as shown in Fig. 30(b). This was because the longitudinally (z) directed momentum in the lower region of the airstream (particularly in the region $0 < y/H < 0.6$) was large enough to overcome the laterally (y) directed momentum, which was produced by the lattice porous core due to its aerodynamic anisotropy. Furthermore, since the lattice porous core, as well as the uniform airstream, were symmetric about the mid-height (i.e., at $y = H/2$) plane parallel to the longitudinal (z) axis, equal amounts of z-directed momentum impinged the core surface in both the lower ($y/H < 0.5$) and upper ($y/H > 0.5$) core regions. Thus, the production of laterally directed momentum (i.e., along the y-axis) was of similar magnitude in both the positive and negative y-directions. In this case, the laterally directed momenta cancelled out, leaving only a significant z-directed momentum component, which resulted in a purely longitudinal traversal of the airstream through the core. This is reflected by the uniformity of the exit velocity profile, shown in Fig. 29, when the lattice porous core was exposed to a uniform incident airstream (i.e., when only the lattice porous core was placed in the wind tunnel's test section).

When the wedge was placed upstream of the lattice porous core, the z-directed momentum flux of the incident airstream was reduced in the lower region ($0 < y/H < 0.6$) due to the separated wake downstream the wedge apex (Fig. 24). This increased hydraulic dispersion within the core because the production of laterally (y) directed momentum was asymmetric about the mid-height plane. When the incident airstream's z-directed momentum is symmetric/asymmetric about the mid-height plane, so too is the production of y-directed momentum by the lattice porous core. Thus, owing to

the core's aerodynamic anisotropy, areas of the incident airstream having large *z*-directed momenta resulted in proportionally large productions of *y*-directed momenta, and vice versa. Following this important property of the lattice porous core, the incident non-uniform airstream was hydraulically dispersed, laterally throughout the core (i.e., lateral dispersion), and the airstream impinged a larger number of fin-functioning ligaments before exiting the core. That is, lateral dispersion causes the airstream to follow a more thermally tortuous [37] path at off-design conditions. Consequently, thermal dispersion, i.e., intensive flow mixing in the vortical wake structures [38] behind the circular ligaments of the core, was augmented. In comparison, thermal dispersion was less effective when the flow merely passed through the core purely longitudinally, e.g., at design conditions. Thus, the thermal performance enhancement of the lattice porous core at off-design conditions was due to its lateral dispersion ability, from which increased thermal dispersion was a natural consequence.

3.3.2 The role of staggered fin-functioning ligaments in thermal dispersion

It was instructive to quantify the effect of circular fin-functioning ligaments on overall heat transfer, for the lattice porous core. For an inline tube bank, without fin-functioning transverse ligaments (Fig. 18(b)), the heat transfer behaviour was not affected significantly by off-design conditions, as shown in Fig. 31(a). Flow over the in-line circular tube bank used in this study was comparable to the correlation reported by Zukauskas [38] which shifted abruptly at Re_D = 1000, due to a corresponding shift in the location of laminar to turbulent boundary layer transition over the fore surface of downstream cylinders, which was caused by growth and interaction with the wake regions of upstream cylinders.

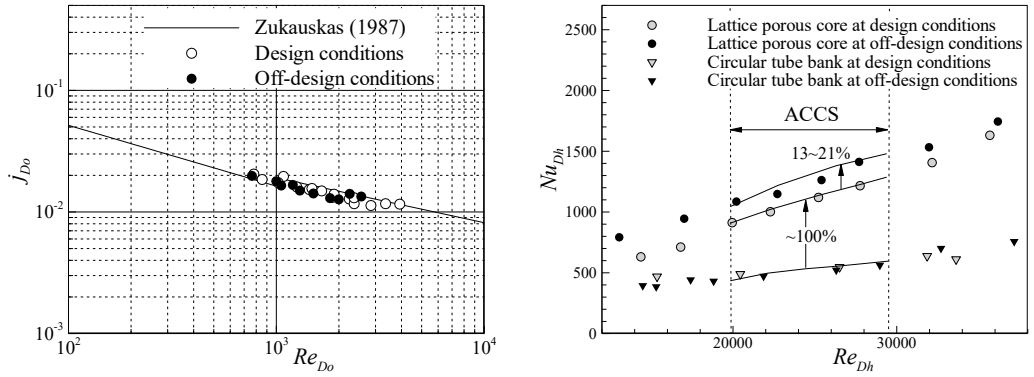
With fin-functioning ligaments, the overall heat transfer performance of the tube bank doubled under design conditions as shown in Fig. 31(b). This was because the heat transfer surface area, as well as thermal dispersion, increased due to the presence of additional circular ligaments. Zhang & Tafti [39] similarly observed changes in the heat transfer performance of louvered fins due to "thermal wake interactions" but these changes depended on several parameters of the louvered fin geometry and in some instances reduced performance.

In the case of the lattice porous core under off-design conditions, the airstream was guaranteed to follow an extended, tortuous, path through several more fin ligaments (relative to that under design conditions) which increased flow mixing within the core. This gave rise to further thermal dispersion and therefore increased (13~21%) convective heat transfer.

3.4 Summary

Due to size constraints on its design, geometrical features inside an ACCS unit were shown to produce a highly non-uniform and obstructed airstream, which exhibited separation and recirculation, incident on a louvered fin-and-tube heater core (Fig. 26). This resulted in a 60% reduction in thermal performance of the heater core, relative to its operation under a uniform and

unobstructed flow (i.e., the design conditions). The thermal performance reduction in this case was found to be significantly larger than that recorded by previous researchers.



(a) (b)

Figure 31. Heat transfer in a lattice porous heater core: (a) Design and off-design thermal performance of a circular tube bank without horizontal fin-functioning ligaments, (b) Contribution of circular fin ligaments to the overall heat transfer in a lattice porous heater core.

Approximately half of the thermal performance reduction was attributed not only to air-flow non-uniformity, as established in the literature, but also to airflow separation immediately upstream of the core. A further performance reduction was attributed to recirculation downstream of the core. However, 10% of the total thermal performance deterioration was still unaccounted for, which could have been due to other minor geometric and fluidic configurational deviations from the design conditions. Precise identification of said deviations were outside the scope of this study, but some examples include unknown flow properties inside the diffuser upstream of the heat transfer section, the effect of an evaporator core upstream of the heater core, and unknown turbulence intensity inside the ACCS unit. These aspects are suggested for future investigations, and they emphasize that various combinations of flow configurations can exist to reduce the thermal performance of practical ACCS units. Indeed, due to the sensitivity of louvered fin-and-tube cores to both upstream and downstream flow configurations, their exact operating environments should be considered during their engineering designs and performance calculations; it is not sufficient to consider individual off-design conditions in isolation, and superimposing their effects is not straightforward.

To increase the thermal performance of ACCS units conventionally employing louvered fin-and-tube cores, subjected to non-uniform incident airstreams, a lattice porous core was developed. The lattice porous core's thermo-fluidic characteristics were compared to those of a louvered fin-and-tube core under both design and off-design conditions (Fig. 30), and it was found that the two cores performed similarly at design conditions, while the lattice porous core showed a performance enhancement at off-design conditions. The louvered fin-and-tube core, instead, showed a performance deterioration at off-design conditions that was qualitatively consistent with the literature. Physically, the behaviour of the lattice porous core is due to hydraulic dispersion, which

is caused by aerodynamic anisotropy inherent in the geometry of the core. It is clear that the thermal performance deterioration of compact air-conditioning systems (such as ACCS units), caused by non-uniform airflow distributions, is not inevitable. In fact, the non-uniform incident flow can be used to significant advantage (Fig. 31(b)).

4 CONCLUSIONS

It has been shown in previous literature that non-uniform flow-fields incident on compact heater cores debilitate their performance. In this work, it has additionally been shown that non-uniform flow-fields are produced by the air intake duct of a typical Automotive Climate Control (ACCS) unit, which causes its enclosed heater core (usually consisting of louvered fins and tubes) to underperform thermally, relative to its designed performance. In particular, this study concluded that:

- The thermal performance of a louvered fin-and-tube core, operating inside a typical ACCS unit, reduces by as much as 60%. It is worth noting that previous researchers have not widely reported on such a drastic performance reduction for louvered fin-and-tube cores operating under any specific conditions deviating from a uniform incident flow field.
- A non-uniform flow field and airflow separation upstream of the louvered fin-and-tube core causes ~30% thermal performance deterioration (i.e., roughly half of the total thermal performance reduction) inside the ACCS unit.
- A recirculation zone downstream of the louvered fin-and-tube core saturates the core's heat transfer capability, resulting in a further 20% thermal performance deterioration inside the ACCS unit.
- 10% of thermal performance deterioration inside the ACCS unit is unaccounted for, and it is speculated that it could have been due to other geometric and fluidic configurational deviations from the design conditions. These deviations were inaccessible for measurement in the current study.
- Several air-conditioning systems may be unique in the non-uniformities they introduce upstream of the heat exchanger core, and it is therefore insufficient to consider previously reported non-uniform flow conditions in isolation. Other contrivances within the air-conditioning system may contribute to further thermal performance deviation. The exact operating conditions must be considered for proper design of the heater core.
- Experimental environments simulating only key ACCS unit geometries help in fluidically understanding the underlying issues related to observed thermal performance deterioration inside a typical ACCS unit. In particular, the louvered fin-and-tube core was found to be incapable of dispersing an incidentally non-uniform airstream, causing only a small portion of the core to be exposed to a cooling airstream that had a suitable velocity for high heat transfer to occur from louver-directed flow within the core.

To improve ACCS thermal performance, a new lattice porous core (consisting of cylindrical tubes with cylindrical fin ligaments attached to each tube) was designed, built, and tested against a conventional louvered fin-and-tube core operating under uniform incident flow, as well as under simulated ACCS environments. It was found that:

- The lattice porous core laterally disperses a concentrated flux of fluid momentum (characteristic of typical non-uniform flow fields encountered in ACCS units), when designed with the correct porosity.
- The lattice porous core performs just as well as a louvered fin-and-tube core under a uniform incident airstream.
- Under a typical non-uniform incident flow field encountered in ACCS units, the lattice porous core exhibits ~15-20% increase in thermal performance, relative to its performance under a uniform incident airstream. In contrast, louvered fin-and-tube cores suffer up to ~30% thermal performance reduction under the same non-uniform incident airstream.
- The mechanism primarily responsible for the lattice porous core's thermal performance enhancement, when subjected to a non-uniform incident airstream, stems from the core's aerodynamic anisotropy which causes lateral dispersion of the non-uniform airstream. Thus, an increased portion of the core's surface area is able to make contact with the airstream as it passes through the core, which increases the overall heat transfer to the airstream.
- Lateral dispersion in the lattice porous core also results in increased thermal dispersion (i.e., intense flow mixing behind the vortical wake structures of the circular fin ligaments) which contributes to the observed thermal performance enhancement.

The results of this study clearly demonstrated that, although compact duct intakes for thermal systems are inevitable, a deterioration of thermo-fluidic performance (e.g., caused by highly non-uniform incident airstreams) can be avoided by allowing the incident coolant stream to be dispersed within the core. Redesign of the core itself, to satisfy the foregoing dispersion requirement, dismisses the need for additional upstream components and/or specialized ducting. Thus, it is ensured that the air-conditioning system remains compact. In this respect, the lattice porous core represents a modular design which is applicable to several A/C systems in general.

5 RECOMMENDATIONS FOR FUTURE WORK

While the lattice porous core developed in the current study represents a suitable proof of concept, it still suffers the drawback of having a complicated and expensive production route. New or existing additive manufacturing methods would need to be developed sufficiently before lattice porous cores can be produced in large enough volumes that are economically profitable.

Pressure drop and acoustic noise considerations were largely out of the current scope of work, but are nonetheless important considerations which impact the power consumption and user satisfaction of ACCS units. As opposed to finding viable manufacturing solutions, the foregoing aspects are suggested for work in the near future, since they may be carried out inexpensively by using numerical simulation tools validated against the data presented herein. Additionally, optimization of the lattice porous core geometry, for various design goals such as reduced weight and increased strength, would be enabled by such numerical simulations.

6 REFERENCES

[1] R. Shah and D. Sekulic, Fundamentals of Heat Exchanger Design, Hoboken, New Jersey: John Wiley & Sons Inc, 2003.

[2] F. Incropera, D. Dewitt, T. Bergman and A. Lavine, Fundamentals of Heat and Mass Transfer, 6th ed., New York: John Wiley & Sons, 2006.

[3] W. Kays and A. London, Compact Heat Exchangers, 3rd ed., New York: McGraw-Hill, 1964.

[4] "What is Climate Control?," Hanon Systems , [Online]. Available: http://www.hanonsystems.com/En/Technology/WhatisClimate#what_tit4. [Accessed 28 August 2022].

[5] F. M. White, Fluid Mechanics, 4th ed., New York: McGraw-Hill, 1998.

[6] H. Schlichting, Boundary Layer Theory, 7th ed., New York: McGraw-Hill, 1979.

[7] F. M. White, Viscous Fluid Flow, 2nd ed., New York: McGraw-Hill, 1991.

[8] W. M. Kays and M. E. Crawford, Convective Heat and Mass Transfer, 3rd ed., New York: McGraw-Hill, 1993.

[9] R. L. Webb and N. H. Kim, Principles of Enhanced Heat Transfer, 2nd ed., New York: Taylor Francis, 2005.

[10] A. Jacobi and R. Shah, "Air-side flow and heat transfer in compact heat exchangers: A discussion of enhancement mechanisms," *Heat Transfer Engineering ,* vol. 19, no. 4, pp. 29-41, 1998.

[11] T. Cowell, M. Heikal and A. Achaichia, "Flow and Heat Transfer in Compact Louvered Fin Surfaces," *Experimental Thermal and Fluid Science ,* vol. 10, pp. 192-199, 1995.

[12] F. Beauvais, "An Aerodynamic look at Automotive Radiators," *SAE Paper No. 650470,* 1965.

[13] C. Davenport, "Heat Transfer and Flow Friction Characteristics of Louvred Heat Exchanger surfaces," in *Heat Exchangers: Theory and Practice*, New York, Hemisphere/McGraw-Hill, 1983, pp. 397-412.

[14] C. T'Joen, M. De Paepe and F. Vanhee, "Heat Exchanger Behaviour in Non Uniform Flow," *Experimental Heat Transfer ,* vol. 19, no. 4, pp. 281-296, 2006.

[15] S. Datta, P. Das and S. Mukhopadhyay, "Obstructed airflow through the condenser of an automotive air conditioner - Effects on the condenser and overall performance of the system," *Applied Thermal Engineering ,* vol. 70, pp. 925-934, 2014.

[16] P. Blecich, "Experimental investigation of the effects of airflow nonuniformity on performance of a fin-and-tube heat exchanger," *International Journal of Refrigeration ,* vol. 59, pp. 65-74, 2015.

[17] M. Kim, B. Youn and C. Bullard, “Effect of inclination angle on the air-side performance of a brazed aluminium heat exchanger under dry and wet conditions,” *International Journal of Heat and Mass Transfer ,* vol. 44, pp. 4613-4623, 2001.

[18] R. L. Webb and P. Trauger, “Flow Structure in the Louvered Fin Heat Exchanger Geometry,” *Experimental Thermal and Fluid Science,* vol. 4, pp. 205-217, 1991.

[19] A. Achaichia and T. A. Cowell, “Heat Transfer and Pressure Drop Characteristics of Flat Tube and Louvered Plate Fin Surfaces,” *Experimental Thermal and Fluid Science,* vol. 1, pp. 147-157, 1988.

[20] N. DeJong and A. Jacobi, “Localized flow and heat tranfer interactions in louvered-fin arrays,” *International Journal of Heat and Mass transfer ,* vol. 46, pp. 443-455, 2003 .

[21] D. K. Tafti, G. Wang and W. Lin, “Flow transition in a multilouvered fin array,” *International Journal of Heat and Mass Transfer,* vol. 43, no. 6, pp. 901-919, 2000.

[22] Y. Chang and C. Wang, “A generalized heat transfer correlation for louver fin geometry,” *International Journal of Heat and Mass Transfer,* vol. 40, no. 3, pp. 533-544, 1997.

[23] M. H. Kim and C. W. Bullard, “Air-side thermal hydraulic performance of multi-louvered fin aluminum heat exchangers,” *International Journal of Refrigeration,* vol. 25, pp. 390-400, 2002.

[24] J. Dong, J. Chen, Z. Chen, W. Zhang and Y. Zhou, “Heat tranfer and pressure frop correlations for the multi-louvered fin compact heat exchangers,” *Energy Conversion and Management ,* vol. 48, pp. 1506-1515, 2007.

[25] P. Shinde and C. Lin, “A heat transfer and friction factor correlation for low air-side Reynolds number applications of compact heat exchangers,” *Science and Technology for the Built Environment ,* vol. 23, pp. 192-210, 2017.

[26] D. Tafti and X. Zhang, “Geometry effects on flow transition in multilouvered fins - onset, propagation, and characteristic frequencies,” *International Journal of Heat and Mass Transfer,* vol. 44, no. 22, pp. 4195-4210, 2001.

[27] K. Bellows, “Flow Visualization of Louvered-Fin Heat Exchangers,” The Air Conditioning and Refrigeration Center, University of Illinois, Urbana, IL, 1997.

[28] J. Kitto and J. Robertson, “Effects of maldistribution of flow on heat transfer equipment performance,” *Heat Transfer Engineering,* vol. 10, no. 1, pp. 18-25, 1989.

[29] L. Henriksson, “Performance of Compact Heat Exchanger in Non-Perpendicular Cooling Airflows,” Chalmers University of Technology, Gothenburg, 2015.

[30] D. Barratt and T. Kim, “Diffuser”. Johannesburg Patent WO/2015/049647, 2015.

[31] C. Kusuda, C. Roper, W. Vannice, A. Muley and K. Maloney, “Micro-Lattice Cross-Flow Heat Exchangers for Aircraft”. Canada Patent CA2836709, 2017.

[32] D. Barratt and T. Kim, “A banked wide-angle diffuser with application to electrostatic precipitators,” *Journal of Power and Energy ,* vol. 229, pp. 88-98, 2014.

[33] T. Kim and T. Lu, “Pressure drop through anisotropic porous mediumlike cylinder bundles in turbulent flow regime,” *Journal of Fluids Engineering ,* vol. 130, p. 104501, 2008.

[34] P. Shinde, “Investigation of Low Reynolds Number Flow and Heat Transfer of Louvered Surfaces,” FIU Electronic Theses and Dissertations, Miami, 2016.

[35] M. Atkins and M. Boer, “Flow Visualization,” in *Application of Thermo-Fluidic Measurement Techniques*, T. Kim, T. Lu and S. Song, Eds., Cambridge, MA, Butterworth-Heinmann, 2016, pp. 15-22.

[36] H. Coleman and W. Steele, Experimentation, Validation, and Uncertainty Analysis for Engineers, 3rd ed., Hoboken, New Jersey: John Wiley & Sons, Inc., 2009.

[37] X. Yang, T. Lu and T. Kim, “Thermal stretching in two-phase porous media: Physical basis for Maxwell model,” *Theoretical and Applied Mechanics Letters,* vol. 3, no. 2, p. 021011, 2013.

[38] A. Zukauskas, “Heat Transfer from Tubes in Crossflow,” *Advances in Heat Transfer,* vol. 18, pp. 87-159, 1987.

[39] X. Xhang and D. K. Tafti, “Classification and effects of thermal wakes on heat transfer in multilouvered fins,” *International Journal of Heat and Mass Transfer,* vol. 44, no. 13, pp. 2461-2473, 2001.